buildings

MDPI

Article

A GPS-Integrated IoT Framework for Real-Time Monitoring of Prefabricated Building Modules During Transportation

Saeid Metvaei [1,*], Alireza Rahimi [2], Hung Cao [2], Sang Jun Ahn [3] and Zhen Lei [1]

[1] Offsite Construction Research Centre, Department of Civil Engineering, University of New Brunswick, Fredericton, NB E3B 5A3, Canada; zhen.lei@unb.ca
[2] Analytics Everywhere Lab, Department of Computer Science, University of New Brunswick, Fredericton, NB E3B 5A3, Canada; alireza.rahimi@unb.ca (A.R.); hcao3@unb.ca (H.C.)
[3] Building Technology Optimization, National Research Council/Government of Canada, Ottawa, ON K1A 0R6, Canada; jun.ahn@nrc-cnrc.gc.ca
* Correspondence: s.metvaei@unb.ca

Abstract

The transportation phase in off-site construction subjects prefabricated modules to road-induced vibrations, shocks, and handling loads that can degrade structural integrity. Existing monitoring approaches often rely on local data loggers, which not only lack real-time visibility but also fail to link structural responses to their precise spatial and temporal context. To address this gap, this study proposes a GPS-integrated Internet of Things (IoT) framework for real-time monitoring of prefabricated modules during transit. The system comprises distributed inertial sensing nodes wirelessly connected to a central gateway, which aggregates and transmits synchronized sensor and GPS data to a cloud platform for analysis and visualization. Field validation demonstrated stable multi-node data acquisition with sufficient battery life to support extended monitoring under LTE connectivity. The framework supports dual-stream analytics: (i) time- and frequency-domain assessment of structural exposure using peak acceleration, RMS, and FFT metrics, and (ii) causal inference of road events (e.g., potholes, bumps, sharp turns). Vertical acceleration emerged as the most responsive diagnostic channel for capturing road-induced excitations, while gyroscope-derived motion profiles distinguish between driver maneuvers and road irregularities. Through seamless integration of structural and geospatial data in a scalable, low-cost system, this framework enables actionable insights for route planning, condition-based inspection, and improved logistics management in modular construction.

Keywords: off-site construction; logistics management; monitoring system; transportation; internet of things (IoT); structural health monitoring (SHM); GPS

Academic Editor: Jurgita Antucheviciene

Received: 4 October 2025
Revised: 13 November 2025
Accepted: 20 November 2025
Published: 24 November 2025

Citation: Metvaei, S.; Rahimi, A.; Cao, H.; Ahn, S.J.; Lei, Z. A GPS-Integrated IoT Framework for Real-Time Monitoring of Prefabricated Building Modules During Transportation. *Buildings* **2025**, *15*, 4242. https://doi.org/10.3390/buildings15234242

1. Introduction

The construction industry, traditionally characterized by labor-intensive practices and vulnerable to various market risks, site uncertainties, and adverse weather conditions [1], is increasingly adopting modular and off-site construction methods. This shift is driven by substantial advantages such as enhanced resource utilization, increased automation capabilities, and improved overall productivity [2,3]. By relocating primary construction activities from on-site environments to controlled factory settings, the construction sector aims to achieve higher environmental sustainability, cost efficiency, improved quality control, and enhanced safety conditions on construction sites [4–7].

In this context, off-site construction broadly refers to the practice of fabricating building modules or their constituent components away from the final installation site [8,9]. Among its various approaches, modular construction represents a prominent subset in which sizable building modules are prefabricated in controlled factory environments and subsequently transported to construction sites for assembly [10]. Nevertheless, transporting these prefabricated modules remains a substantial logistical challenge, potentially undermining the benefits intended by modular construction methods [11]. After fabrication, each module undergoes multiple logistics operations, including transportation, typically via flatbed tractor-trailers, and repetitive loading and unloading processes before being positioned on pre-prepared foundations or temporarily stored through stacking [11,12].

Throughout these operations, modules are exposed to a variety of uncertain and dynamic loads, such as mechanical shocks, vibrations, and stresses induced by uneven road surfaces, wind forces, or improper handling during driving and craning activities [13]. Such conditions may induce structural anomalies, potentially manifesting as visible defects, underlying cracks, or alignment deformations [14]. These structural defects not only compromise the integrity of the modules but can also lead to a range of downstream consequences, including rejection or rework at the site, increased material and labor expenditures, disruptions to Just-in-Time (JIT) schedules, project delays, and latent safety risks during installation and service life [12,15,16].

Research has demonstrated that most structural damages originate from logistics-related operations [11,14]. Among these operations, vibration-induced impacts during transportation present greater risks to structural integrity compared to other logistical phases, such as lifting or storage [17]. Empirical investigations highlight that vertical accelerations during transit can reach up to 32 m/s^2 (3.3 g), a level comparable to floor accelerations observed in low-rise reinforced concrete buildings during near-fault earthquakes of magnitude Mw 5.5 to 8.0, highlighting the intense mechanical stresses involved in transportation [13,18]. Furthermore, horizontal acceleration shocks resulting from sudden braking or road surface irregularities amplify these impacts, reinforcing the need for continuous monitoring during haulage. However, monitoring mobile structures, where both the structure and the impacting loads are simultaneously in motion, poses significant challenges due to environmental variations or operational vibrations that can confound conventional damage analysis methods, which are designed primarily for stationary structures [19,20].

To mitigate these challenges, recent research trends have leveraged Internet of Things (IoT) sensing to track transport-induced responses in real time. Central to these IoT-based frameworks are various sensing technologies, such as accelerometers and gyroscopes, that measure the magnitude and frequency of linear and angular motions [21]. These devices can be deployed individually or in conjunction with other sensors like strain gauges, which provide critical data on mechanical deformations [22]. For instance, Valinejadshoubi et al. [12] used accelerometers for continuous vibration logging in modular transport, Song et al. [23] employed a commercial ShockLog to measure tilt, roll, and impacts in volumetric units, and Khayam et al. [22] demonstrated a portable, multi-sensor platform combining accelerometers and strain gauges for precast elements.

While these studies underscore the potential of sensor-based monitoring, their practical deployment remains constrained by several limitations. Many systems rely on localized data logging, which postpones damage assessment until after delivery, reducing opportunities for timely corrective action [22]. Furthermore, the spatial heterogeneity of modular structures necessitates deploying multiple sensors per unit to achieve comprehensive monitoring coverage [24], which complicates large-scale use due to challenges in time synchronization, system integration, power management, and cost. Addressing these

limitations, Arshad and Zayed [14] proposed a multi-sensing architecture that streams accelerometer, gyroscope, and strain data from distributed wireless nodes to a cloud platform in real time. However, their system remains disconnected from broader logistics systems, lacking continuous positional context and event-level metadata, which limits real-time tracking and contextual interpretation of structural responses [25].

In parallel, GPS technology has become foundational to off-site logistics, with widespread integration into IoT platforms to support real-time tracking and operational visibility during prefabrication transport [26–30]. Beyond these core applications, researchers have also explored GPS integration for lean coordination [31], fleet optimization [32], and carbon-emission monitoring [33]. However, despite this progress, GPS data streams continue to operate separately from structural health monitoring systems. This lack of integration inhibits the ability to correlate structural responses with specific roadway or handling/driving conditions. As a result, critical opportunities are missed for proactive route optimization, adaptive transport strategies, and transparent traceability across the logistics chain [34].

To address this gap, the present study introduces a scalable, integrated, and real-time monitoring framework that combines distributed IoT-based inertial sensing with GPS-enabled geospatial tracking. The system couples low-cost, battery-powered sensing nodes and a cellular gateway with cloud-based storage and visualization, ensuring resilient multi-node data acquisition even under intermittent connectivity. This unified architecture enables geo-tagging of structural anomalies, continuous localization of modules in transit, and route-specific assessment of environmental and logistical stressors. Beyond data collection, the framework supports two complementary analytics: (i) structural impact assessment through time- and frequency-domain vibration analysis, and (ii) causal event inference that attributes anomalies to roadway conditions or driver maneuvers. By bridging the gap between structural monitoring and location intelligence, the proposed system advances a data-driven methodology that enhances safety, enables predictive damage assessment, and supports proactive logistics management in modular construction workflows.

The remainder of this paper is organized as follows. Section 2 reviews prior studies and systems for monitoring prefabricated modules in transit and identifies the gaps this work seeks to address. Section 3 describes the proposed IoT architecture, including hardware, firmware, and communications/data pipelines, while Section 4 evaluates its performance in terms of throughput, signal stability, power consumption, and connectivity. Section 5 describes the deployment and analysis workflow for structural impact assessment and causal event attribution; and Section 6 presents and interprets the monitoring results, illustrating the system's diagnostic capabilities. Finally, Section 7 concludes with key contributions, limitations, and directions for future research.

2. Literature Review

This section structures the literature discussion around three interrelated dimensions that collectively define a systems-oriented perspective for in-transit monitoring of prefabricated modules: what to measure, how to sense it, and where existing approaches fall short. Section 2.1 addresses what to measure by synthesizing prior studies on structural responses and transport-induced events to identify the key monitoring parameters and diagnostic features relevant to off-site logistics. Section 2.2 explores how to sense it, reviewing both commercial and custom IoT-based solutions and highlighting prevailing architectural patterns and their limitations in mobile, multi-node data acquisition environments. Finally, Section 2.3 identifies unresolved gaps, particularly the weak connection between struc-

tural data and geospatial context, which motivates the development of the GPS-integrated, multi-node IoT framework introduced in the following sections.

2.1. Monitoring Structural Responses and Transport Events

Reliable monitoring of prefabricated building modules during transit begins with understanding how transport events translate into measurable structural responses. Structural Health Monitoring (SHM) provides the foundation for this analysis by integrating sensor-based systems and analytical techniques to evaluate structural integrity in real time or at scheduled intervals [35]. In modular construction, SHM is especially vital due to the additional stresses and potential damage that prefabricated modules experience during transportation and handling [13]. Timely detection of structural anomalies is essential to prevent costly repairs, assembly delays, and operational disruptions upon site arrival [15].

A wide range of SHM techniques has been studied, including strain-based, vibration-based, acoustic emission, guided wave, and vision-based techniques [35,36]. Among these approaches, active methods such as guided waves or acoustic emissions, while effective in static settings, are less suitable for the dynamic and non-stationary environment of module transport [20,37]. Similarly, vision-based methods also face practical limitations during transit due to motion blur, changing illumination, and high processing demands [35]. For in-transit applications, techniques that measure direct mechanical responses, particularly strain and vibration, are more practical. Strain-based approaches, which employ resistive strain gauges or fiber-optic sensors, provide localized and precise measurements of deformation under stress [16,35]; however, their limited coverage and installation complexity reduce their application in finished modules [38]. Vibration-based monitoring, on the other hand, captures global responses through accelerometers and gyroscopes, making it more suitable for detecting damage or abnormal loading during transportation [39,40]. Nevertheless, its reliance on global signals constrains its capacity for precise damage localization.

Beyond the selection of monitoring techniques, the effectiveness of SHM systems depends heavily on the analytical methods used to interpret sensor data. For strain data, researchers often employ direct strain profile tracking or time-domain statistical analysis. Gómez et al. [38], for instance, monitored strain evolution across time and spatial locations, validating observed trends against a simplified two-dimensional finite element model (FEM) to confirm their qualitative accuracy. For vibration data analysis, non-model-based approaches, particularly time- and frequency-domain analyses, are widely adopted as they avoid the computational complexity of physics-based models [12,41]. For example, Fast Fourier Transform (FFT) analysis has been applied to accelerometer and gyroscope data to identify shifts in dominant frequencies as indicators of stiffness loss [14], while peak accelerations and root-mean-square (RMS) metrics have been used to quantify vibration intensity during transport [12,22]. Machine learning models, including hybrid deep learning architectures, have also been tested to predict damage severity from multi-sensor data [16]. However, despite their potential, such data-driven approaches require extensive, diverse training datasets that are rarely available for modular transport scenarios. This highlights the need for lightweight, portable, and high-resolution acquisition systems that operate reliably in real-world transport and help build the diverse datasets required for data-driven models.

Alongside SHM, vehicular perception research, particularly event detection, has emerged as a complementary line of research, aiming to identify the sources of structural responses. Accelerometers and gyroscopes, often combined with GPS and other onboard sensors, have been widely employed to infer vehicular events ranging from road anomalies (e.g., potholes, bumps, cracks) to driving behaviors (e.g., braking, sharp turns, lane

changes) [42–44]. A variety of techniques have been applied for this purpose, including threshold-based detection, time-series alignment methods, and machine learning classifiers [45]. For example, Khandakar et al. [46] demonstrated that vertical acceleration and pitch rotations are strongly associated with speed bumps, roll responses are indicative of potholes, and yaw signals reflect steering actions, making threshold-based analysis of these axes effective for identifying such events. While these approaches have been validated in the context of vehicular dynamics and road-quality assessment, they have rarely been extended to modular construction. Bridging this gap by correlating structural responses with specific causal events enables more interpretable monitoring outcomes and offers actionable route-based insights and greater accountability in modular transport operations.

2.2. IoT-Based Sensing Frameworks for In-Transit Monitoring

Recent studies have developed portable sensing systems to monitor stresses on prefabricated modules during transportation [12,14,22,23]. Typical configurations employ accelerometers for vibration measurement, gyroscopes or inclinometers for rotational tracking, and strain gauges for localized deformation assessment [35]. Song et al. [23], for example, demonstrated a commercial data-logging system equipped with tri-axial accelerometers and tilt sensors that differentiated stresses such as lateral roll, longitudinal tilt, vibrations, and shocks. While effective, such commercial solutions are prohibitively expensive and operate as independent units, each with separate control and communication modules. This complexity limits scalability and makes deployment across multiple sensing points within a module impractical [14].

To address cost and integration challenges, researchers have explored the development of custom microcontroller-based alternatives. For instance, Khayam et al. [22] developed a multi-metric monitoring device for precast delivery that combined a microcontroller, accelerometer, strain gauge channels, and local SD storage. Similarly, Valinejadshoubi et al. [12] employed distributed Arduino-based units with accelerometers to capture vibrations at 125 Hz. Although these systems reduced hardware costs by using low-cost off-the-shelf components, their reliance on local data storage hindered real-time monitoring, constrained scalability, and delayed anomaly detection until after transit.

The adoption of Internet of Things (IoT) frameworks has further advanced this field by enabling distributed sensing nodes to wirelessly transmit data to a central unit and onward to cloud platforms for real-time analysis and visualization [14,47]. A key design consideration in such systems is the choice of wireless communication protocol, which must balance throughput, latency, power efficiency, and reliability over the long distances encountered in transportation. Low-Power Wide-Area Networks (LPWAN), such as LoRa and LoRaWAN, provide long-range, energy-efficient connectivity [48,49], but cannot support continuous high-frequency IMU data streaming due to restricted throughput [50]. By contrast, cellular technologies such as LTE and emerging 5G offer higher data rates and wide coverage, making them more suitable for transit monitoring at the cost of higher power demands [50]. Using this approach, Arshad and Zayed [14] developed an IoT-integrated multi-sensor system that combined IMU and strain sensing in compact wireless units, transmitting downsampled data to a central gateway and then to a remote server via LTE. However, this system was validated only in laboratory conditions, leaving real-world deployment challenges in logistics settings largely unaddressed.

Despite these advances, a critical gap remains: most IoT-based SHM systems treat structural and geospatial data in isolation. While GPS has been widely adopted in offsite construction logistics, enabling real-time tracking of module location, arrival time prediction, and proactive route management [34,51,52], its integration with structural

monitoring has been largely overlooked. Coupling GPS data with structural responses (and their causal inference) would provide valuable spatiotemporal insights, such as linking transportation events to specific road segments, identifying problematic transport routes, and correlating handling events with structural anomalies. Such integration would not only enhance accountability and enable targeted inspections but also support predictive logistics strategies, representing a major step toward holistic monitoring of modular transportation operations.

2.3. Knowledge Gap

Despite recent advances in IoT-based monitoring for modular construction, critical limitations continue to hinder scalability, responsiveness, and diagnostic effectiveness. Most existing solutions, whether commercial or based on low-cost microcontrollers, operate as standalone sensing units with local data storage, which postpones anomaly detection, complicates synchronization, and obstructs fleet-level visibility. Furthermore, research into LTE-enabled sensing systems remains narrow in scope and largely untested under real-world transport conditions, where communication reliability, power constraints, and mobility pose significant challenges. Structural health monitoring and geospatial tracking technologies have also evolved in silos, often failing to integrate high-frequency IMU data with continuous positional information. This disconnect makes it difficult to attribute structural responses to specific transport events or route segments, undermines the interpretability of sensor data, and isolates monitoring insights from broader logistics planning. Addressing these gaps necessitates a low-cost, real-time, and field-tested IoT framework capable of multi-node deployment, robust wireless communication, and seamless fusion of structural and geospatial data to support actionable, event-aware transport diagnostics.

3. IoT-Enabled Transport Monitoring System for Offsite Logistics

To achieve the objectives outlined above, this study presents an IoT-based system designed for real-time, distributed data acquisition. The system simultaneously collects vibration data from multiple points on the prefabricated module and visualizes this information through a cloud-based dashboard, supporting structural impact monitoring as well as inspection and route planning decisions. The proposed system adopts a layered architecture, integrating a distributed network of Sensing Nodes (SNs) and a centralized Gateway Node (GN). This structure aligns with the three-layer IoT model proposed by Lv et al. [53], which comprises the perception, communication, and application layers. In the context of this system:

- The SNs constitute the perception layer, capturing real-time inertial data that reflects the dynamic behavior of prefabricated modules during transportation.
- The GN operates within the communication layer, aggregating data from multiple SNs and transmitting it to a remote server.
- At the application layer, a cloud-based dashboard ingests, processes, and visualizes the data, enabling both the detection of transportation-induced impacts and their geospatial visualization on an interactive map.

The remainder of this section details the hardware components associated with each system layer, followed by an overview of their firmware logic and end-to-end data flow, emphasizing how these design choices address the research gaps identified earlier.

3.1. Hardware Configuration

3.1.1. Sensing Node (Perception Layer)

Each Sensing Node (SN) is a compact, battery-powered prototype built using off-the-shelf components and custom wiring on a perfboard. Designed for distributed mounting

on prefabricated modules, the nodes capture in-transit motion data while meeting key requirements such as cost-effectiveness, flexibility, and uninterrupted operation during long-distance transport.

As shown in Figure 1, the core of each SN is an ESP32-C6 development board, which integrates a low-power microcontroller with Wi-Fi 6 and Bluetooth 5. It was chosen for its energy efficiency and reliable wireless performance, particularly its support for the ESP-NOW protocol used for inter-device communication in this system. Additionally, each SN collects motion data via an MPU6050 sensor module, which combines a 3-axis accelerometer and a 3-axis gyroscope, enabling high-rate tracking of acceleration and angular velocity.

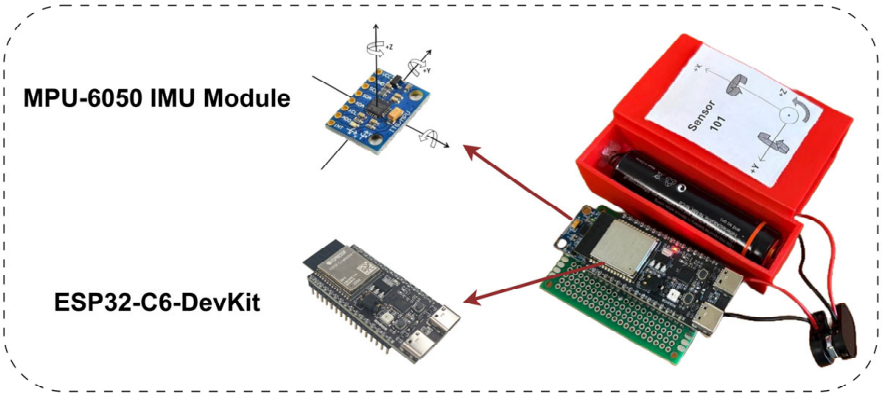

Figure 1. Sensing node prototype with ESP32-C6 development board and MPU6050 inertial module for six-DoF motion tracking.

Each node is powered by a 3000 mAh rechargeable Li-ion cell, providing sufficient runtime for extended monitoring. All components, including the controller, sensor, and power interface, are compactly arranged and manually soldered onto a perfboard, then enclosed in a 3D-printed case, resulting in a compact yet reconfigurable sensing prototype.

3.1.2. Gateway Node (Communication Layer)

The Gateway Node (GN) serves as the central aggregator and communication bridge between the distributed sensing nodes (SNs) and the cloud. It receives data streams from multiple SNs, geotags them, stores them locally, and simultaneously forwards them to the cloud, enabling synchronized, geo-tagged data acquisition and full data integrity even during connectivity losses.

As shown in Figure 2, the GN is implemented using a multi-functional IoT development board that integrates an ESP32-WROVER microcontroller with the SIM7600G-H cellular module. This configuration supports low-power local communication with SNs via ESP-NOW, long-range data transmission over LTE, and real-time positioning via GPS. A micro-SD data logger is also included in the board for local data storage, ensuring data retention during network outages.

To support extended deployment under real-world transport conditions, the GN is powered by a 15,000 mAh external power bank, reducing the need for frequent recharging and ensuring continuous operation. All components, including the development board and power supply, are housed in custom-designed 3D-printed enclosures that provide mechanical protection and ensure stable performance in mobile environments.

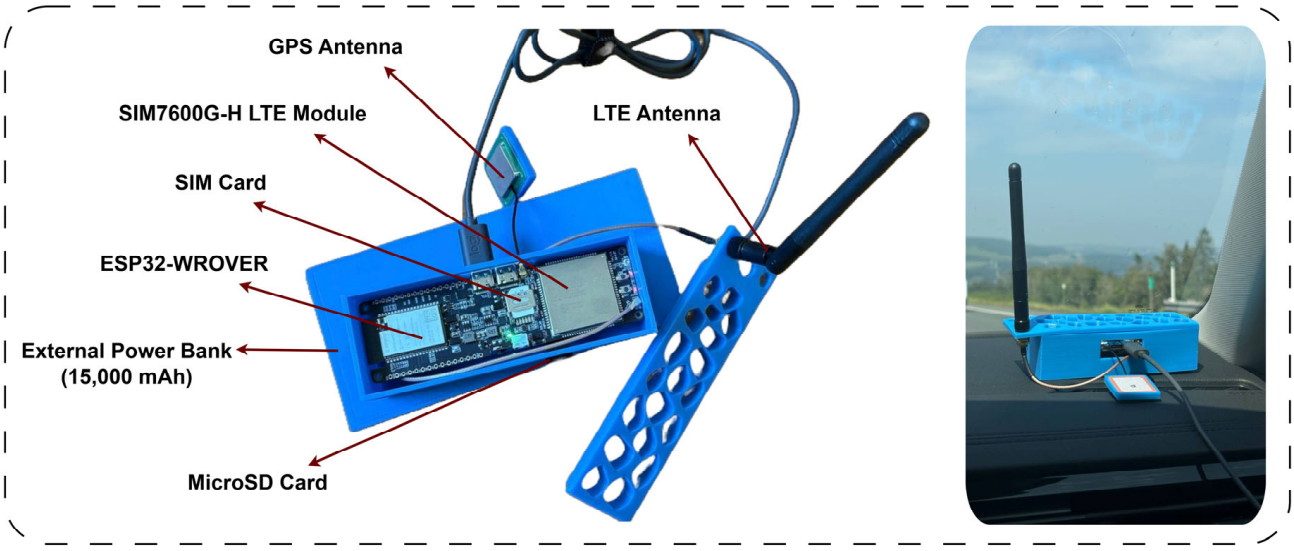

Figure 2. Gateway node prototype integrating ESP32-WROVER, SIM7600G-H LTE/GPS module, external antenna, microSD storage, and power bank.

3.1.3. Cloud/Application Environment (Application Layer)

The cloud environment is hosted on a high-performance virtual machine (VM) configured to manage concurrent data streams and multi-node communication. The deployed stack integrates InfluxDB for storing time-series data, Grafana for real-time dashboards and visualization, an MQTT broker for managing data exchange between the gateways and the cloud, and Python 3.10 applications for processing and organizing incoming information. External access is secured through Cloudflare, which manages DNS, encryption, and basic threat protection. Together, this setup provides a scalable, reliable, and secure backbone that transforms raw sensor and GPS streams into synchronized, spatially aligned, module-referenced, and session-organized datasets, producing actionable insights for real-time monitoring and post-trip assessment of transport-induced impacts and their causal events.

3.2. System Logic and Data Flow

3.2.1. Overview of System Logic

The proposed software stack supports distributed data acquisition, resilient aggregation, and real-time cloud-based visualization. Figure 3 presents the end-to-end data flow and the key protocols across system layers. During operation, multiple SNs are mounted on a prefabricated module, each continuously collecting inertial data from onboard sensors. These measurements are batched and wirelessly transmitted to the GN via the ESP-NOW protocol. The GN buffers incoming packets, appends GPS coordinates, and forwards the packets to the cloud via 4G LTE. This pipeline supports both live visualization and post-transport analysis, enabling continuous monitoring of structural responses and detailed post-transport assessment.

To support scalable deployment, the system includes automated startup routines at both the edge and cloud levels. Upon initialization, the GN briefly broadcasts a Wi-Fi access point, allowing nearby SNs to request configuration parameters such as time synchronization, sampling rate, and batch size. This eliminates the need to modify SN firmware when parameters change and ensures consistent data synchronization across nodes.

At the cloud level, users initiate a monitoring session through a web interface by specifying the observation period and the participating devices (GN and SNs). All incoming data from these devices within the specified time window is tagged with a unique session

ID, streamlining data organization and supporting simultaneous tracking of multiple transport events. The following subsections further describe the specific firmware logic implemented within each system component.

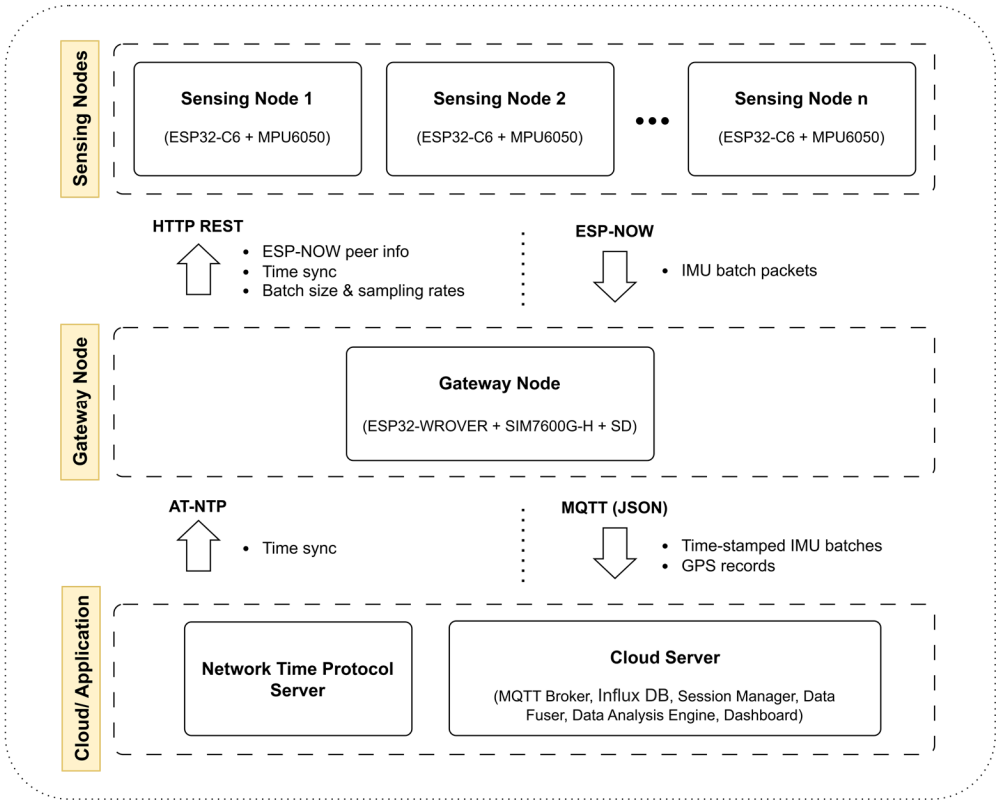

Figure 3. Data flow and communication protocols in the proposed IoT system.

3.2.2. Firmware Logic on Sensing Nodes

Figure 4 illustrates the firmware workflow implemented on each SN, comprising two main stages: initialization and a main operational loop. During initialization, the SN connects briefly to the GN over Wi-Fi to receive configuration parameters such as time sync, sampling rate, and batch size. It then switches to ESP-NOW mode and registers the GN as its peer. The IMU sensor is also initialized and calibrated using zero-offset values.

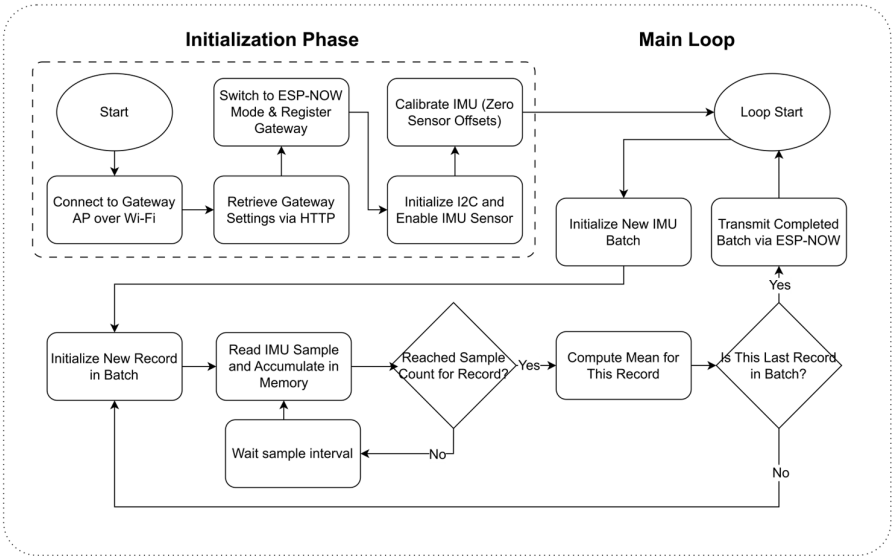

Figure 4. Firmware workflow on Sensing Nodes.

In the operational loop, the SN collects acceleration and angular velocity data at a native rate of 100 Hz. These readings are temporarily stored and averaged over a fixed number (as specified by the GN's parameters) to reduce noise and data volume. This approach ensures reliable, real-time transmission and efficient data handling while maintaining measurement accuracy [54]. The downsampled data is then compiled into a transmission batch. Once the batch reaches its defined size, it is sent to the GN via ESP-NOW. The buffer is then cleared, and the cycle repeats.

3.2.3. Firmware Logic on Gateway Node

Figure 5 illustrates the GN's firmware workflow, which manages real-time data reception from SNs and ensures reliable transmission to the cloud. Upon startup, the GN initializes its main component and synchronizes its clock with a network time server to maintain accurate timestamps. It also activates a temporary Wi-Fi access point to share configuration data with nearby SNs, enabling their flexible setup without manual coding.

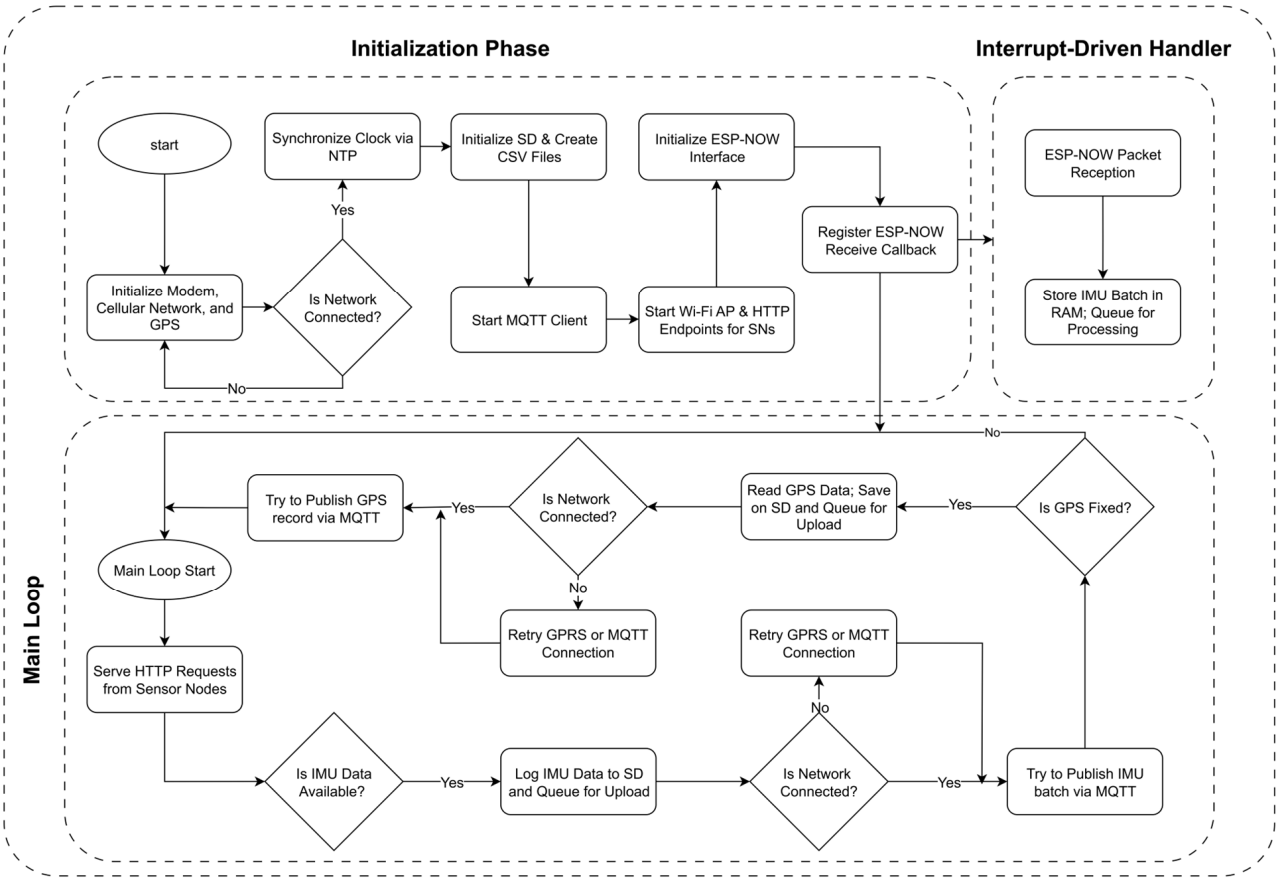

Figure 5. Firmware workflow on Gateway Node.

Following initialization, the GN operates two concurrent processes: (i) an interrupt-driven callback for receiving IMU data, and (ii) a main loop that reads GPS data and publishes IMU/GPS packets to the cloud. In the event of network unavailability, the data will be buffered locally in memory for deferred upload. Simultaneously, all data is logged to a micro-SD card to ensure no loss during disconnections. These mechanisms enable low-latency acquisition, reliable transmission, and resilience in mobile or intermittently connected environments.

3.2.4. Cloud/Application Workflow

The cloud workflow begins with initiating a recording session via a web interface. Each session is defined by its time window, assigned gateway, and associated sensing nodes. The mounting orientation of each SN is also recorded to align IMU readings within a consistent global reference frame for both the module and the vehicle [45]. This session-based approach supports concurrent data collection from multiple gateways across different transport routes, ensuring scalability and avoiding interference.

During an active session, a cloud-hosted MQTT broker receives data packets from gateways. A Python application validates each packet, assigns the session ID, and adjusts sensor axes based on mounting metadata to maintain spatial consistency. The processed data is then stored in InfluxDB, a time-series database optimized for high-frequency data. For real-time monitoring, Grafana connects directly to InfluxDB, providing interactive plots of inertial and GPS data, along with a live transport map. Real-time metrics, such as RMS, are computed using Flux queries, enabling immediate visualization of vibration intensity. Advanced analyses, including frequency-domain evaluation and causal event detection, are performed offline in Python. This end-to-end pipeline ensures synchronized, spatially aligned sensor data and real-time insight into transport conditions, supporting both daily monitoring needs and deeper analytical objectives.

4. System Validation and Performance Evaluation

4.1. Data Throughput Capacity

This section evaluates the data flow across the system to establish a reliable and sustainable transmission rate. The first communication layer, between the sensing nodes and the gateway, uses the ESP-NOW protocol, which supports a maximum payload of approximately 250 bytes per unencrypted packet [55]. Based on the data structure, each IMU record occupies 16 bytes, while each batch includes an additional 6 bytes for metadata (e.g., batch ID and sensor ID). Although the theoretical limit allows up to 15 IMU records per batch, this study conservatively caps each batch at 10 records to ensure transmission reliability.

In the second communication layer, where the gateway transmits data to the cloud via MQTT, the practical payload limit is approximately 1 KB. Given that a single IMU batch of 10 records, once serialized into JSON format, can exceed 500 bytes, it is more efficient to publish only one batch per MQTT message to maintain performance and reliability. In comparison, serialized GPS data averages around 220 bytes, which remains well within acceptable limits for transmission.

To validate this configuration, a test was conducted with three active sensing nodes, each recording at an effective rate of 10 Hz (downsampled from 100 Hz) and transmitting data in batches of 10 records. Over a 40 min session under stable LTE conditions, no data loss was observed, confirming the system's reliability under these settings. However, although this configuration prioritizes stability, the system is technically capable of handling higher data rates, as ESP-NOW supports up to 50–100 messages per second, and the GN's MQTT client can be tuned to handle a comparable transmission rate if higher-frequency operation is required.

4.2. Signal Stability Assessment

To evaluate baseline signal stability and characterize sensor noise, a sensing node was placed in a controlled, static environment with minimal external disturbances. Under these conditions, any variation in sensor output is attributed primarily to intrinsic noise in the accelerometer and gyroscope. The results, illustrated in Figure 6a,b, show over two hours of continuous measurements. For the accelerometer operating in the ± 2 g

range, the observed RMS noise was approximately 0.001 g, with most readings fluctuating between −0.003 g and 0.005 g. The calculated standard deviation of the acceleration signal was 5 mg, which aligns closely with the typical noise characteristics of the MPU6050 sensor as specified in the manufacturer's datasheet (≈3 mg) [56] and as observed experimentally by Manso and Bezzeghoud (≈4 mg) [57]. In comparison, Khayam et al. [22] reported a lower standard deviation of 1.2 mg using the ADXL354 sensor. This difference can be attributed to the ADXL354's higher resolution and lower intrinsic noise, approximately sixteen times better than the MPU6050 [57,58].

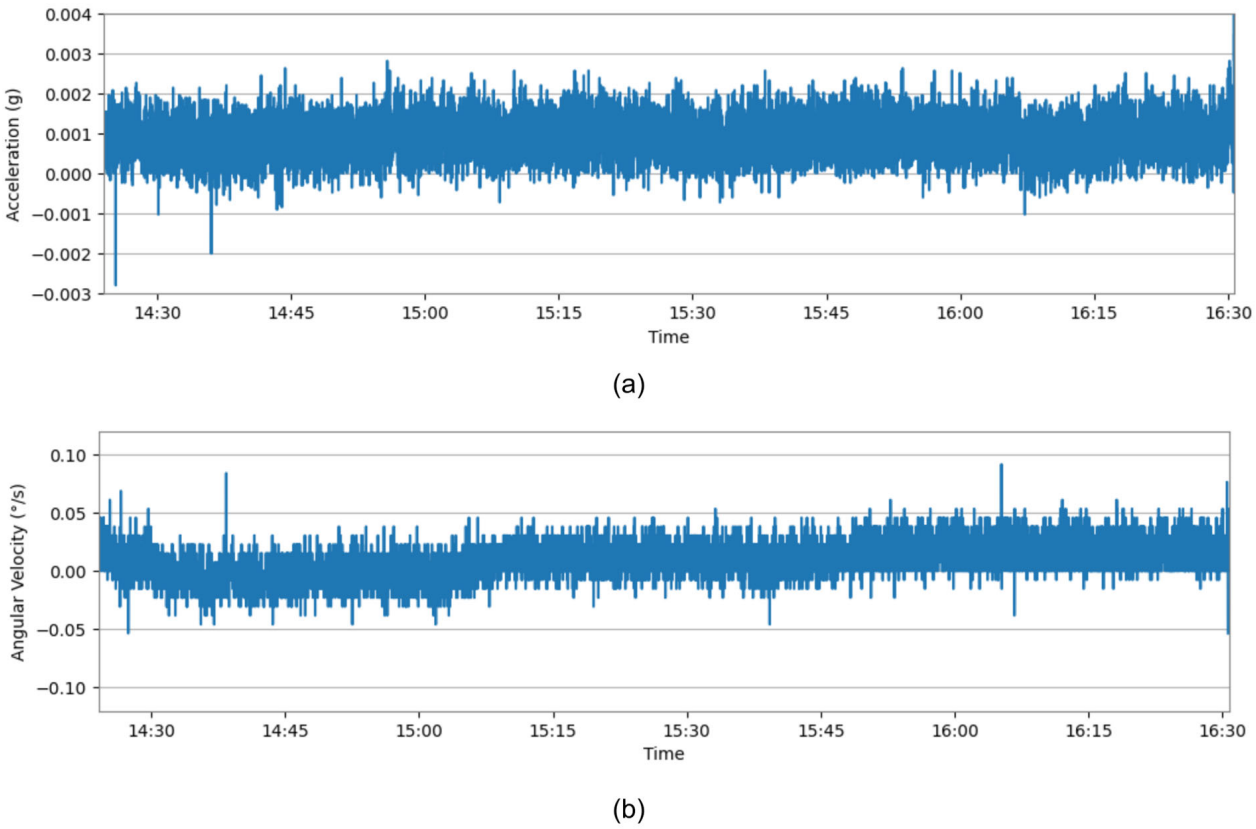

Figure 6. IoT sensing system performance tests under static conditions: (**a**) Acceleration noise, (**b**) Angular Velocity/Gyroscope noise.

Similarly, for the gyroscope operating within the ±25°/s range, the observed RMS noise was 0.01°/s, with readings typically varying between −0.0°/s and 0.0°/s. These observations are consistent with the expected noise density of the MPU6050 (0.03–0.0°/s) [56]. This agreement confirms that the sensing module operates within its expected range and provides stable, low-noise outputs suitable for reliable vibration-based monitoring.

4.3. Power Consumption

A power consumption analysis was conducted using a power profiler to assess the energy efficiency of the system components under typical operating conditions. For the sensing nodes, the average current draw (adjusted to reflect the 5 V output from a 3.7 V source) was measured at 123 mA while sampling under the settings described in Section 4.2. For the gateway node, operating concurrently with three active sensing nodes, the current consumption was recorded at approximately 245 mA. This is higher than the 165 mA reported by Khayam et al. [22], which is expected since the current system integrates on-board wireless communication and an LTE cellular module for real-time cloud data transmission, features that inherently increase power demand.

As a 3000 mAh Li-ion battery powers each SN, and the GN is supported by a 15,000 mAh external power bank, their battery life could be estimated using Equation (1) [59]:

$$Battery\ Life = \frac{Battery\ Capacity}{I} \times 0.8 \quad (1)$$

where I represents the measured current, and the 0.8 correction factor accounts for real-world inefficiencies such as temperature, aging, and voltage sag. Based on these calculations, each SN is expected to operate for approximately 19 h, while the GN can sustain operation for about 2 days. These runtimes are sufficient to support uninterrupted monitoring of prefabricated modules during typical transport operations.

4.4. Network Connectivity and System's Resilience

To assess the system's real-world connectivity and robustness, a full-scale field test was conducted during a 10 h, 800 km road trip from Fredericton, New Brunswick, to Montreal, Quebec. The experimental setup included two SNs transmitting vibration data to the GN, which relayed both sensor and GPS data to the cloud in real time via LTE. As shown in Figure 7, the full travel route is illustrated on the map with communication gaps highlighted in red circles. A total of 13 disconnections were observed throughout the trip. The average disconnection time was around 15 s, with the longest outage lasting 25 s. Overall, the cumulative duration of untransmitted data due to temporary LTE loss was less than five minutes, accounting for less than 1% of the total monitoring period.

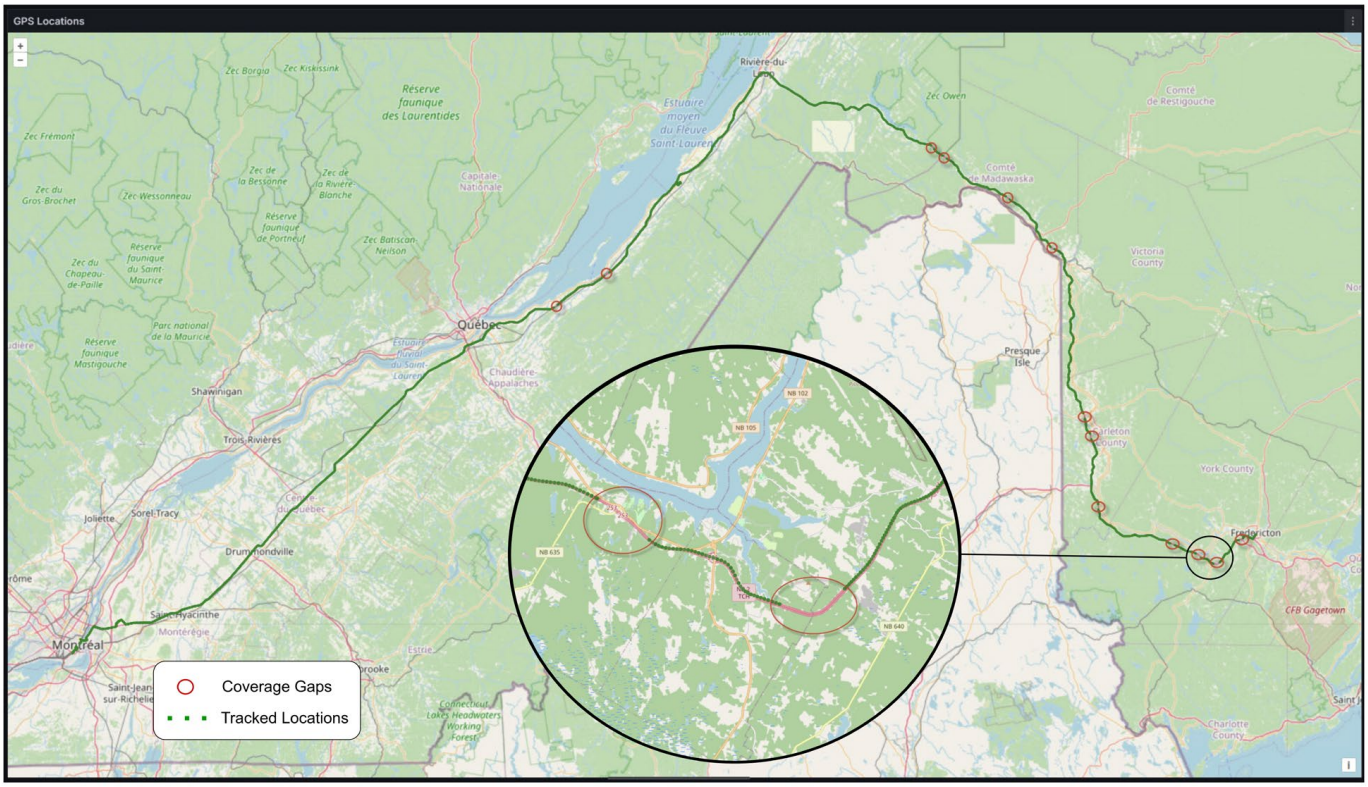

Figure 7. Real-time GPS tracking of an 800 km test route, highlighting tracked locations (green line) and network coverage gaps (red circles), with a black circle displaying a magnified view of specific route details.

These results demonstrate the effectiveness of the system's resilient data handling strategy. During connectivity loss, the GN firmware maintains in-memory data queuing and executes continuous reconnection attempts, which substantially minimizes real-time data loss. Moreover, all records are concurrently written to the onboard SD card, ensur-

ing complete post hoc recovery and lossless data integrity in scenarios where real-time transmission is interrupted.

Further geospatial analysis of the data reveals that most connectivity gaps occurred in rural areas of New Brunswick, which aligns with third-party carrier coverage maps such as nPerf, indicating limited 4G availability and fallback to 3G or weaker signals in certain regions. In contrast, the road network within Quebec Province, particularly along major highways, maintained consistent 4G connectivity, resulting in uninterrupted cloud transmission across the latter part of the route. In practice, this suggests that coverage maps can be used to anticipate connectivity risks and adjust buffering strategies accordingly, while also demonstrating the system's reliability in urban corridors with stable 4G coverage.

5. Application of the Proposed IoT Framework

To validate the applicability of the proposed IoT sensing framework, a controlled field experiment was carried out under representative transportation conditions. The system was deployed to monitor a modular unit in transit, capturing transportation-induced impacts together with their causal events, such as road irregularities and driver maneuvers. These capabilities are critical for enabling targeted inspection and maintenance immediately upon arrival, reducing the risk of undetected damage propagating into later construction stages. In addition, the collected dataset offers valuable evidence for refining module design practices, supporting the development of units that are more resilient to transportation-induced stresses and better suited to off-site construction logistics. The system also enables quantitative benchmarking of ride quality across transport options and suspension/tie-down configurations (e.g., air-ride flatbeds versus trailer bogies), informing evidence-based selection of transport methods to reduce transport-induced loads on the module.

5.1. Experimental Setup

While the system is designed for full-scale prefabricated housing modules, this proof-of-concept test used a reduced-scale wooden box to emulate structural behavior during transit. The test module consisted of a lightweight timber-framed box with approximate dimensions of $700 \times 500 \times 400$ mm^3 and a total mass of ~30 lbs. This design mirrors similar experimental testbeds used in prior modular transport studies, such as those by Arshad et al. [16], and balances physical representativeness with ease of deployment. Two SNs were affixed to the structure, one at the floor and another vertically mounted on a side wall, to enable distributed inertial monitoring and capture both translational and rotational movements across the module. Data acquisition settings followed the configuration described in Section 4.1, with raw inertial data sampled at 100 Hz and downsampled to 10 Hz.

To simulate actual hauling conditions, the module was securely placed inside the trunk of a personal SUV and restrained to avoid internal shifting. The GN board was also placed on the vehicle dashboard, ensuring an unobstructed GPS signal and reliable LTE connectivity while serving as the central aggregator for the SN data. A test session was initiated through the cloud session manager, where metadata such as time, duration, and SNs deployment configuration were registered. The local axes of the SNs were reoriented in the session manager to match the vehicle's global reference frame, allowing acceleration and angular velocity to be interpreted in terms of longitudinal (Y), lateral (X), and vertical (Z) axes, along with derived roll, pitch, and yaw angular motions.

The experiment spanned approximately 80 min (12:00–13:20) and was conducted under mixed urban driving conditions in Fredericton, New Brunswick. The route encompassed typical city driving characteristics, including well-maintained pavement, moderate accelerations and braking, and speeds below 50 km/h, interrupted by short stationary

periods at red lights and parking stops. To ensure broader coverage, the drive also incorporated segments over degraded pavement and brief stretches of rural roads with higher speed limits, thereby capturing a more comprehensive range of vibrational inputs. During the trip, a field observer manually annotated specific events, such as speed bumps and potholes, to enable post hoc validation of sensor-based detections. This experimental design provided a controlled yet realistic environment for evaluating the framework's effectiveness in impact detection, causal event inference, and the added value of GPS integration, laying the foundation for the application scenarios discussed in the following sections.

5.2. Analytical Methods for Modular Transport Assessment

The proposed framework enables two complementary analytical streams, structural impact assessment and causal event inference, that together provide a holistic understanding of the module's dynamic experience during transportation. Structural impact assessment quantifies the module's dynamic response to vibrational and impact loads, while causal event inference attributes these responses to specific roadway features or driver maneuvers. This combined approach supports real-time diagnostics, post-transport verification, and informed decision-making for logistics and maintenance.

5.2.1. Structural Impact Assessment

This analysis focuses on identifying and characterizing the vibrational loads that act on the module during transit. To achieve this, both time-domain and frequency-domain techniques are employed in a complementary manner.

In the time domain, two key metrics are utilized:

- Peak Amplitude Detection: Identifies short-duration, high-magnitude spikes in acceleration that may correspond to shocks or impacts capable of compromising structural integrity. This enables near real-time flagging of potentially damaging events.
- Root Mean Square (RMS) Analysis: Provides a smoothed measure of vibration energy over sliding time windows, establishing a baseline for motion severity and allowing continuous tracking of cumulative vibrational exposure throughout the journey.

The frequency-domain perspective extends this analysis by applying Fast Fourier Transform (FFT) to reveal the spectral distribution of energy within the signal. Dominant frequency components and recurring vibration patterns can be linked to periodic excitations, such as repetitive road undulations, or to resonant responses that may indicate loosened connections or progressive structural degradation. This dual perspective ensures that both transient shocks and sustained vibrational behaviors are captured and interpreted accurately.

5.2.2. Causal Event Inference

To complement structural response analysis, the framework performs causal event inference to identify the external triggers of detected vibrations, such as road surface irregularities and driver-induced maneuvers. By analyzing characteristic patterns in acceleration and angular velocity, the system enables the detection of events such as speed bumps, potholes, sharp turns, etc. When integrated with GPS trajectories and vehicle speed, these detections can be spatially validated against roadway features and temporally linked to driver actions, thereby improving transparency and traceability in transportation monitoring. In addition, to evaluate the feasibility of automated event detection without manual annotation, a rule-based heuristic pipeline was examined, successfully capturing the majority of observer-noted events while highlighting areas for further research. This causal attribution capability is crucial for improving transport safety and efficiency, as it allows

fleet managers and engineers to identify hazardous routes, optimize driving practices, and prioritize inspection efforts for modules subjected to elevated dynamic loading.

6. Monitoring Results and Discussion

During the field experiment, the deployed IoT framework successfully delivered real-time sensor feedback from the modular test unit to the cloud dashboard. The dashboard streamed raw accelerometer and gyroscope measurements from the distributed sensing nodes alongside GPS-based location tracking and transportation speed, enabling continuous monitoring of the module during transit. In addition, preliminary metrics such as sliding-window RMS values were computed online to support immediate interpretation of vibration intensity and to flag abnormal fluctuations during operation. More advanced analyses, including FFT and causal event inference, were conducted post hoc to demonstrate the framework's diagnostic potential and could be integrated into the dashboard in future iterations.

Figure 8 presents the GPS trajectory of the experimental route, accompanied by vehicle speed and altitude profiles, confirming uninterrupted data collection across the monitoring session. The corresponding time-series accelerometer and gyroscope outputs from sensing node #1 are shown in Figure 9a, capturing the module's dynamic responses during the experiment. As expected, during stationary intervals, horizontal accelerations along the x- and y-axes approached zero, while the vertical *z*-axis stabilized near 1 g due to gravitational alignment. Minor deviations from these nominal values are attributed to sensor mounting tolerances or uneven ground conditions while parked.

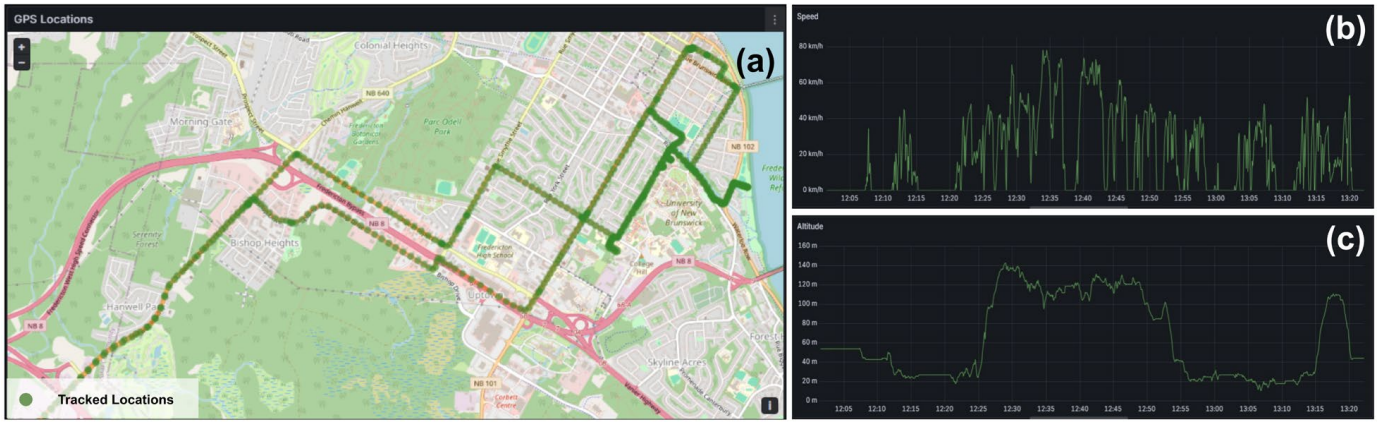

Figure 8. GPS trace of the experimental route (**a**) with corresponding vehicle speed (**b**) and altitude (**c**) profiles.

The gyroscope records (Figure 9b) reveal limited rotational motion about pitch and roll (approximately $\pm 15^\circ/\text{s}$ and $\pm 22^\circ/\text{s}$, respectively), consistent with the damping effects of modern suspension systems that mitigate excessive body tilt. By contrast, yaw exhibited more pronounced fluctuations, reaching up to $\pm 35^\circ/\text{s}$, reflecting the vehicle's deliberate steering maneuvers and directional changes. These trends highlight the system's ability to distinguish between structural responses to road-induced perturbations (pitch and roll) and driver-controlled maneuvers (yaw), underscoring the diagnostic potential of multi-axis motion sensing for modular transport monitoring.

6.1. Structural Impact Assessment

Building on the analytical methods introduced in Section 5.2, this section presents the results of time-domain and frequency-domain analyses used to evaluate the system's ability to detect transportation-induced impacts. The combined use of peak acceleration,

RMS metrics, and FFT provides both immediate event detection and insight into the overall vibrational environment experienced by the module during transit.

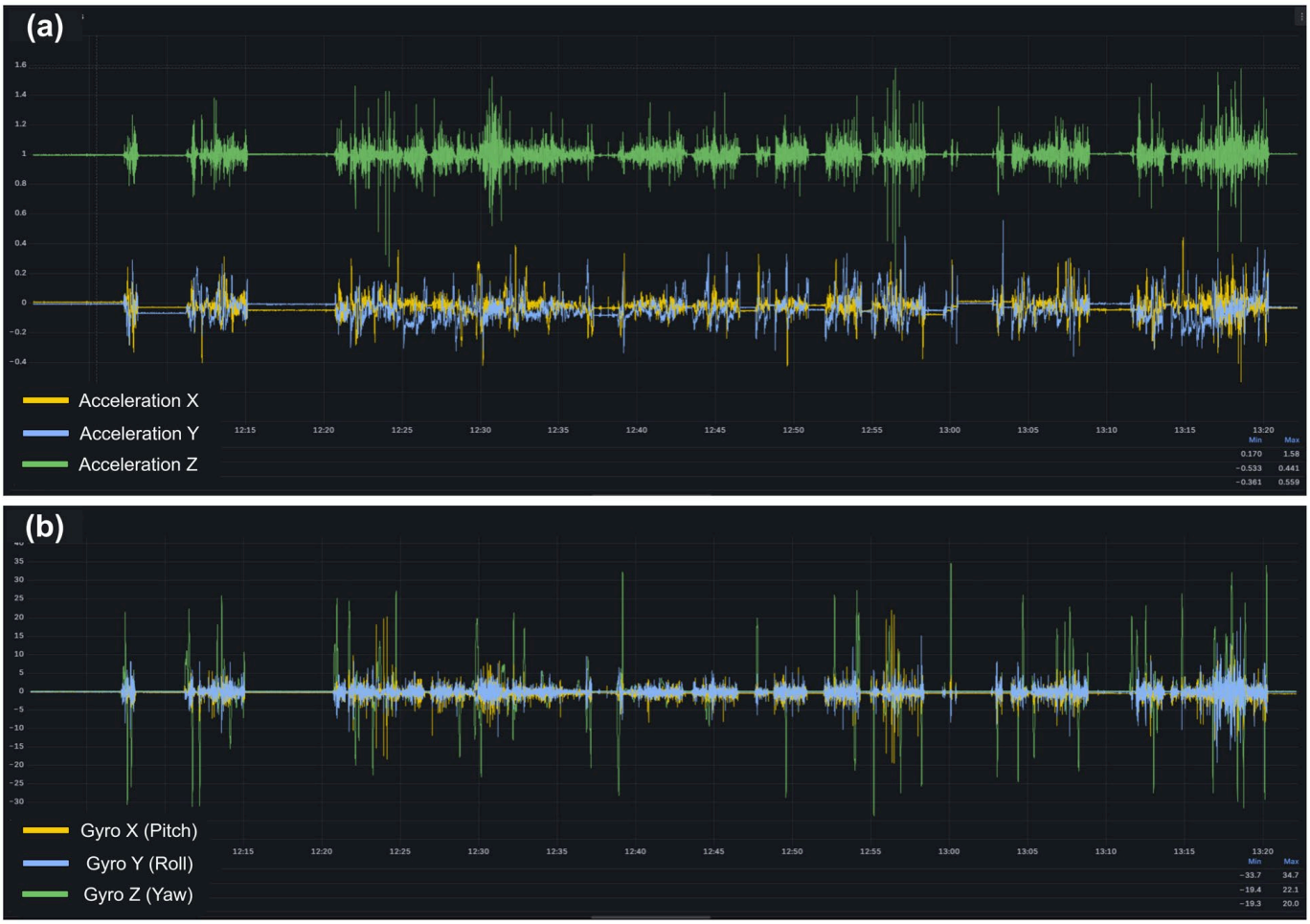

Figure 9. Real-time data trend of (**a**) Acceleration, and (**b**) Gyro/Angular Velocity during the trip.

6.1.1. Peak Acceleration

Peak acceleration analysis was performed to detect high-magnitude transient events by applying upper and lower threshold bounds to the vertical acceleration (*Z*-axis) data. Values exceeding these bounds were flagged as shocks or impacts with the potential to compromise the structural integrity of the prefabricated module. Threshold selection was guided by prior studies: Godbole et al. [13] recommend designing modular units to withstand vertical accelerations of up to 3.3 g beyond gravity, whereas Innella et al. [60] reported that most vertical accelerations on local roads at speeds near 40 km/h remain within ±0.63 g. Based on these benchmarks, this study adopted conservative limits of +1.6 g (upper) and +0.4 g (lower) to reliably capture significant vibration spikes while filtering out routine fluctuations.

As shown in Figure 10, the module experienced vertical accelerations outside these limits at three distinct points along the route. Analysis of GPS data revealed that the first two instances (Figure 10a) occurred at the same roadway location during two separate passes, where three consecutive speed bumps were present. A close-up of the acceleration profile at 12:56, combined with the corresponding GPS trace, confirms these anomalies as the source of the shocks. The third exceedance occurred at 13:17 within a parking lot characterized by poor pavement quality and multiple potholes (Figure 10b). Here, the vertical acceleration exhibited a pronounced energy spike, confirming the presence of severe surface irregularities. A closer inspection of vehicle speeds at these points further

contextualizes these events: the speed bumps were traversed at speeds exceeding 25 km/h, while the pothole impacts occurred at approximately 17 km/h. This coupling of inertial and geospatial data provided by the system highlights not only the detection of shocks but also their contextual interpretation in relation to road conditions and driving habits.

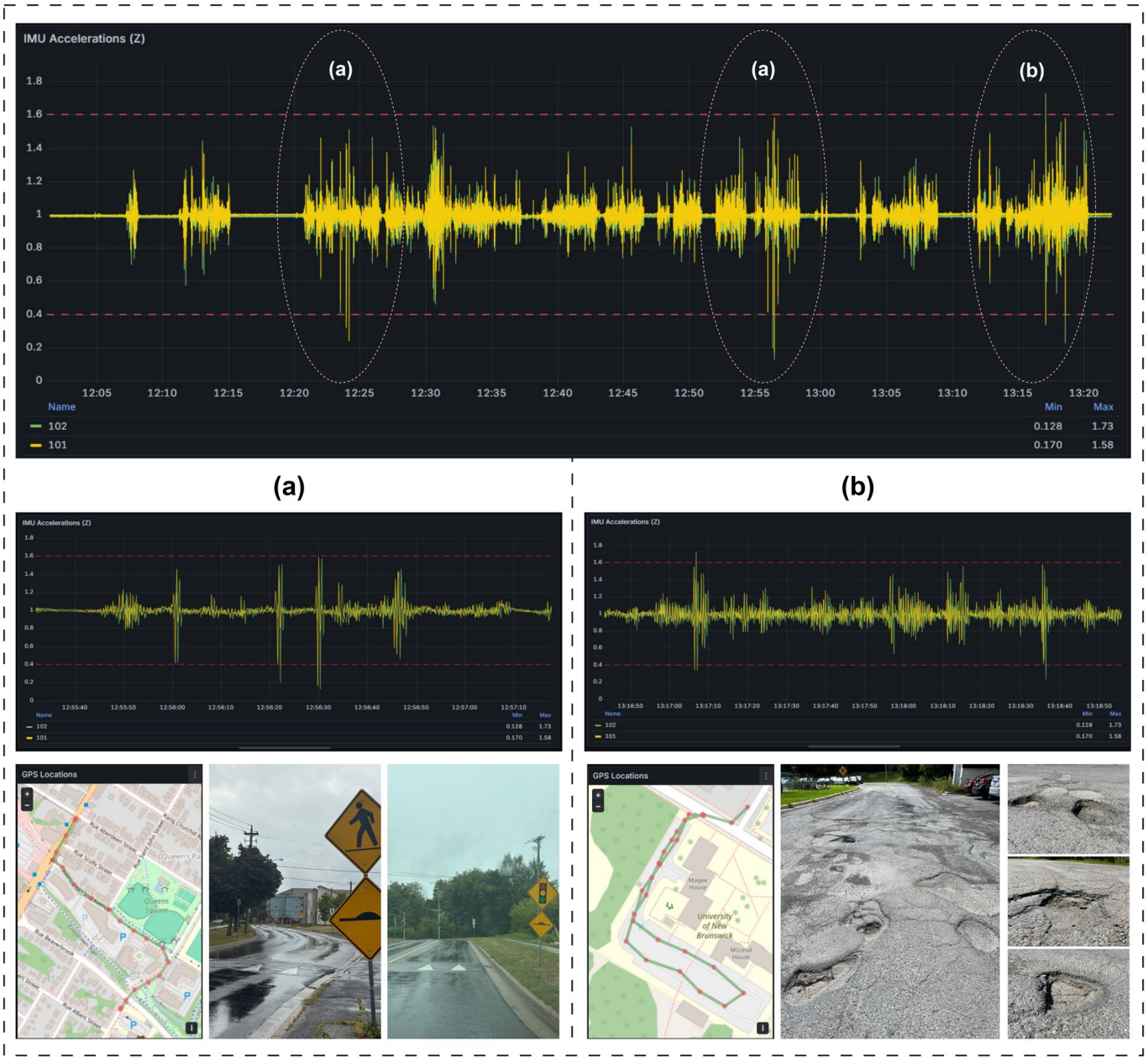

Figure 10. Vertical acceleration (*Z*-axis) exceedances detected by thresholding, with GPS traces and site photos confirming (**a**) speed bumps and (**b**) pothole-induced shocks.

Regarding sustained vibration intensity, the maximum vertical acceleration recorded during the monitored session was 0.84 g, with a standard deviation of 42.4 mg. These values are in line with those reported by Khayam et al. [22], who documented a maximum of 0.68 g and an SD of 48.6 mg over a similar 80 min transport duration. Although the two studies differ fundamentally in terms of vehicle type and monitored structure, the consistency in acceleration magnitudes reinforces the validity and reliability of the proposed monitoring system.

In contrast to the vertical direction, threshold values for lateral and longitudinal accelerations are less clearly defined in the literature, as these directions are generally considered less critical for modular stability [60]. However, regulatory standards specify minimum performance requirements of 0.8 g forward deceleration and 0.5 g lateral and rearward acceleration for securement systems [61]. In this experiment, inertial data in all non-vertical directions remained below these regulatory limits, indicating that the module was not exposed to excessive inertial loads in the horizontal plane during the monitored session.

6.1.2. Root Mean Square

RMS acceleration is a key indicator of the overall energy content of a vibration signal and serves as a reliable metric for assessing the sustained severity of dynamic loading [12]. Higher RMS values generally correspond to more intense or prolonged vibrational exposure, which may contribute to material fatigue or joint degradation over time. In the proposed framework, RMS is continuously computed using a 10 s sliding window and visualized in real time on the monitoring dashboard, enabling trend analysis and immediate detection of abnormal vibrational behavior during transportation.

Figure 11 shows RMS traces for the lateral (X) and longitudinal (Y) axes recorded by the two sensing nodes. The results clearly differentiate between periods of movement and stationary intervals. During parked phases, RMS values flatten near zero, with minor offsets attributable to uneven ground or sensor mounting imperfections. The close alignment of the two nodes (yellow and green traces) across both axes indicates stable calibration and effective synchronization, validating the reliability of the sensing system. In the lateral direction, the RMS signal is characterized by isolated spikes, which correspond to short-duration impacts from lane changes or turning maneuvers. By contrast, the longitudinal RMS exhibits more sustained elevations, reflecting repeated acceleration, braking, and road gradient variations typical of urban driving conditions. Together, these patterns demonstrate how RMS trends capture both discrete and continuous vibrational phenomena relevant to modular transport assessment.

Figure 11. RMS acceleration in the (**a**) lateral (X) and (**b**) longitudinal (Y) directions for both sensing nodes.

For the vertical (Z) axis, RMS analysis was conducted following a preprocessing step to eliminate the static gravitational component, which otherwise dominates the signal and obscures dynamic variations. In this study, the mean value within each window was subtracted from the raw acceleration records, effectively transforming the RMS into the standard deviation of the vertical signal. This approach isolates the true dynamic content of the motion and enhances sensitivity to road-induced shocks [22,62].

As shown in Figure 12, the resulting RMS-Z trace after DC removal exhibits a sequence of distinct peaks aligned with road anomalies and surface irregularities. Notably, the spikes at 12:56 and 13:17 correspond to the high-energy shocks previously identified in Figure 10, representing speed bumps and potholes, respectively. The latter exhibits a higher energy level, reflecting the severity of the pavement degradation in that location. During stationary intervals, the vertical RMS converges near zero, validating the effectiveness of the bias removal step and confirming that the remaining signal content represents actual vibrational input. Overall, the system's real-time calculation of vertical RMS provides a reliable indicator of excitation events and a practical means of quantifying structural exposure during transit.

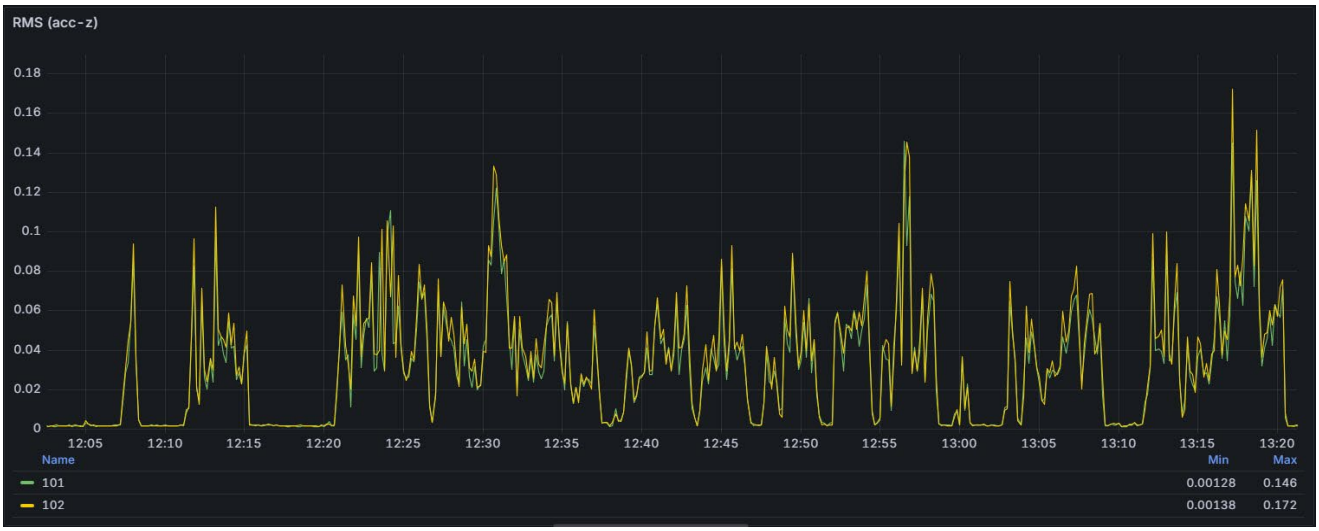

Figure 12. RMS acceleration in the vertical (Z) direction after DC removal.

6.1.3. Fast Fourier Transformation

To complement time-domain metrics, a frequency-domain analysis was conducted using the FFT to examine the spectral content of the acceleration and gyroscope signals. The FFT identifies dominant frequency components that characterize the dynamic response of the module during transport. Changes in dominant frequencies or energy distributions across axes and sensing locations may indicate structural alterations or evolving boundary conditions, making frequency-domain analysis a valuable diagnostic tool [14,63].

Figure 13 shows the FFT spectra for the six degrees of freedom measured by SN #1, with stationary periods excluded and mean bias removed to isolate dynamic vibrations. Both lateral (X) and longitudinal (Y) accelerations exhibit prominent peaks concentrated near 0 Hz. These low-frequency components reflect gradual vehicle maneuvers such as steering corrections, braking, and acceleration. Superimposed on this low-frequency baseline, the *X*-axis also shows scattered peaks in the 1–3 Hz range, representing discrete, event-driven shocks, while the *Y*-axis displays a smoother spectrum consistent with sustained vibrational exposure, patterns that correspond with the RMS trends reported earlier.

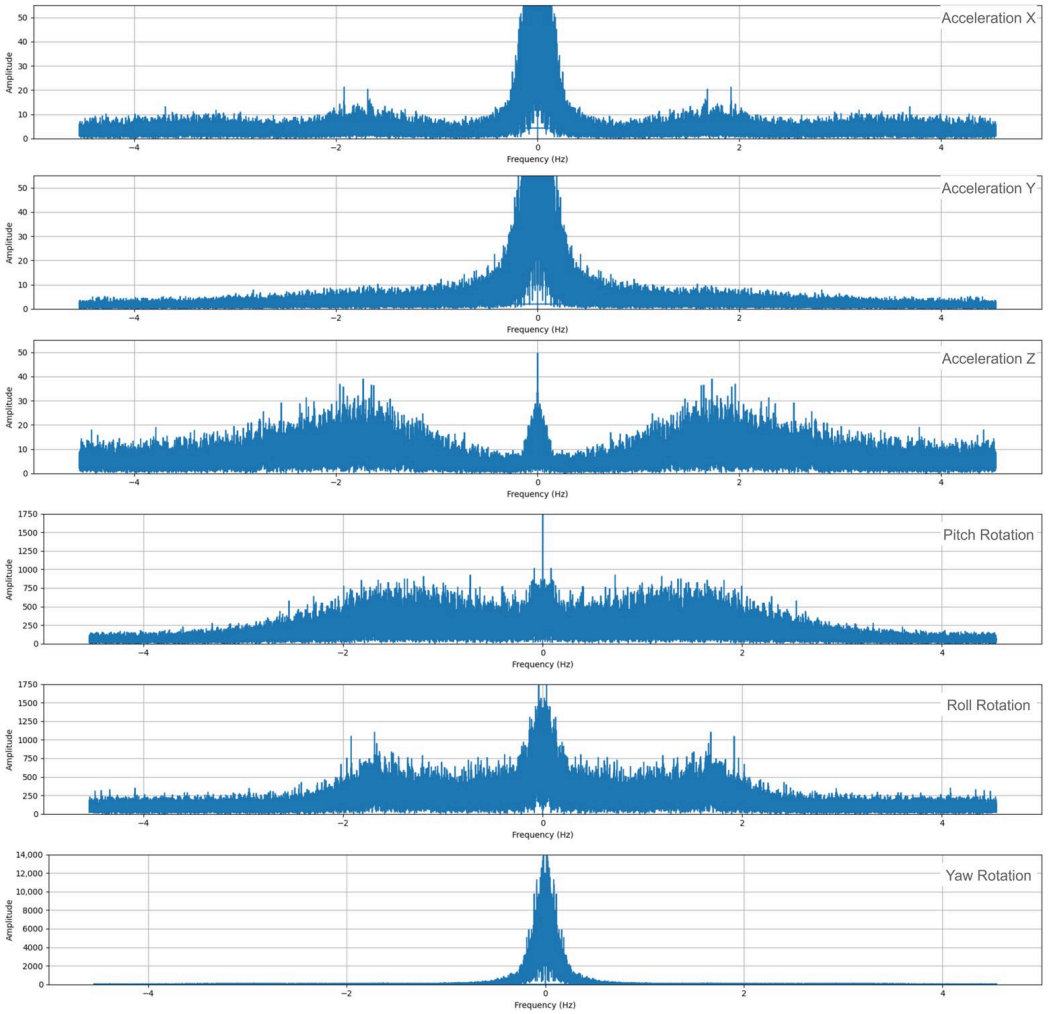

Figure 13. FFT spectra of acceleration and rotational responses for SN #1.

In contrast, the vertical (Z) acceleration spectrum shows broader peaks spanning 0.7–3 Hz, identifying this axis as the most sensitive diagnostic channel for road-induced impacts. The wider frequency band indicates a combination of periodic excitations from the vehicle suspension system and random vibrations transmitted from road surface irregularities. Moreover, these vertical dynamics are strongly coupled with pitch and roll rotational responses, as expected when the vehicle traverses uneven surfaces. Such a multi-axis dynamic response, particularly from heave, pitch, and roll channels, has been shown to exacerbate shipment damage more severely than vertical motion alone [64].

When comparing pitch and roll, the roll spectrum exhibits more distinct frequency components than pitch, likely suggesting that roll-inducing events, such as potholes, are more abrupt, while pitch tends to be influenced by more gradual excitations, such as speed bumps. In contrast, the yaw spectrum displays a narrow, dominant peak near 0 Hz, attributable to slow steering maneuvers. This confirms that yaw is governed primarily by driver input rather than by road-induced impacts.

Because FFT plots contain complex and sometimes overlapping features, complementary statistical indicators were extracted to quantify spectral characteristics across both sensing nodes. Table 1 summarizes the third quartile (Q3), standard deviation (SD), and spectral centroid for each signal. The Q3 highlights significant dominant frequency magnitudes, SD characterizes the spread of spectral energy, and the centroid identifies the frequency at which most energy is concentrated [14,65]. The results confirm that vertical accelerations show a relatively concentrated distribution of high-energy vibration signals

(lowest SD, highest centroid, and elevated Q3 among the accelerations), reinforcing their role as the primary diagnostic channel for detecting transportation-induced excitations. Additionally, the close agreement between SN #1 and SN #2 further validates system reliability and demonstrates consistent measurement performance across distributed nodes.

Table 1. Statistical indicators of FFT magnitudes for both sensing nodes.

Measurement/Sensing Unit		SN #1	SN #2
Acceleration X	Third Quartile (Q3)	5.303	5.065
	Standard Deviation	9.847	9.881
	Spectral Centroid	1.537	1.55
Acceleration Y	Third Quartile (Q3)	4.194	3.973
	Standard Deviation	14.155	14.424
	Spectral Centroid	0.983	1.008
Acceleration Z	Third Quartile (Q3)	9.452	10.458
	Standard Deviation	4.739	5.219
	Spectral Centroid	2.189	2.221
Pitch Rotation	Third Quartile (Q3)	265.462	284.263
	Standard Deviation	148.225	137.317
	Spectral Centroid	1.629	1.903
Roll Rotation	Third Quartile (Q3)	249.536	256.386
	Standard Deviation	160.752	150.802
	Spectral Centroid	1.632	1.698
Yaw Rotation	Third Quartile (Q3)	70.29	68.994
	Standard Deviation	922.16	931.72
	Spectral Centroid	0.442	0.44

6.2. Causal Event Inference

Beyond quantifying structural impacts, inertial data can also be leveraged to infer the causal events that generate these responses. Specifically, characteristic IMU signal patterns allow discrimination between road-surface anomalies (e.g., speed bumps, potholes) and driving maneuvers (e.g., turns, lane changes, braking). Prior studies demonstrate that traversing over bumps and potholes induces distinctive signatures across both accelerometer and gyroscope channels: speed bumps typically excite vertical accelerations accompanied by pronounced pitch rotations (rotation about the lateral *X*-axis), while potholes introduce abrupt vertical drops coupled with roll rotations (rotation about the longitudinal *Y*-axis) [46]. These trends are endorsed by the collected experimental data. Figure 14 illustrates the response of SN #1 during two representative events: (a) a speed bump at 12:56 and (b) a pothole at 13:18, both previously identified in Figure 10. Although both pitch and roll responded in each case, pitch motion dominated in the bump event while roll motion dominated in the pothole, supporting their utility as diagnostic features for automatic event flagging.

Unlike pitch and roll, yaw rotation (rotation about the vertical *Z*-axis) is largely decoupled from road irregularities and instead reflects steering input. According to Chen et al. [42], a positive yaw rate indicates a left turn, while negative values reflect rightward steering. Figure 15 shows the yaw response during a driving sequence through a roundabout, aligned with GPS traces from points (a–e). The yaw profile captures each maneuver, starting with a lane change, followed by entry, circulation, exit, and a final right turn, demonstrating the framework's ability to geolocate steering events and correlate them with roadway features. By integrating speed and lateral acceleration, already captured within the system, these analyses can be extended to reliably detect unsafe behaviors such as aggressive cornering, thereby enhancing causal inference and improving transparency in off-site transportation monitoring.

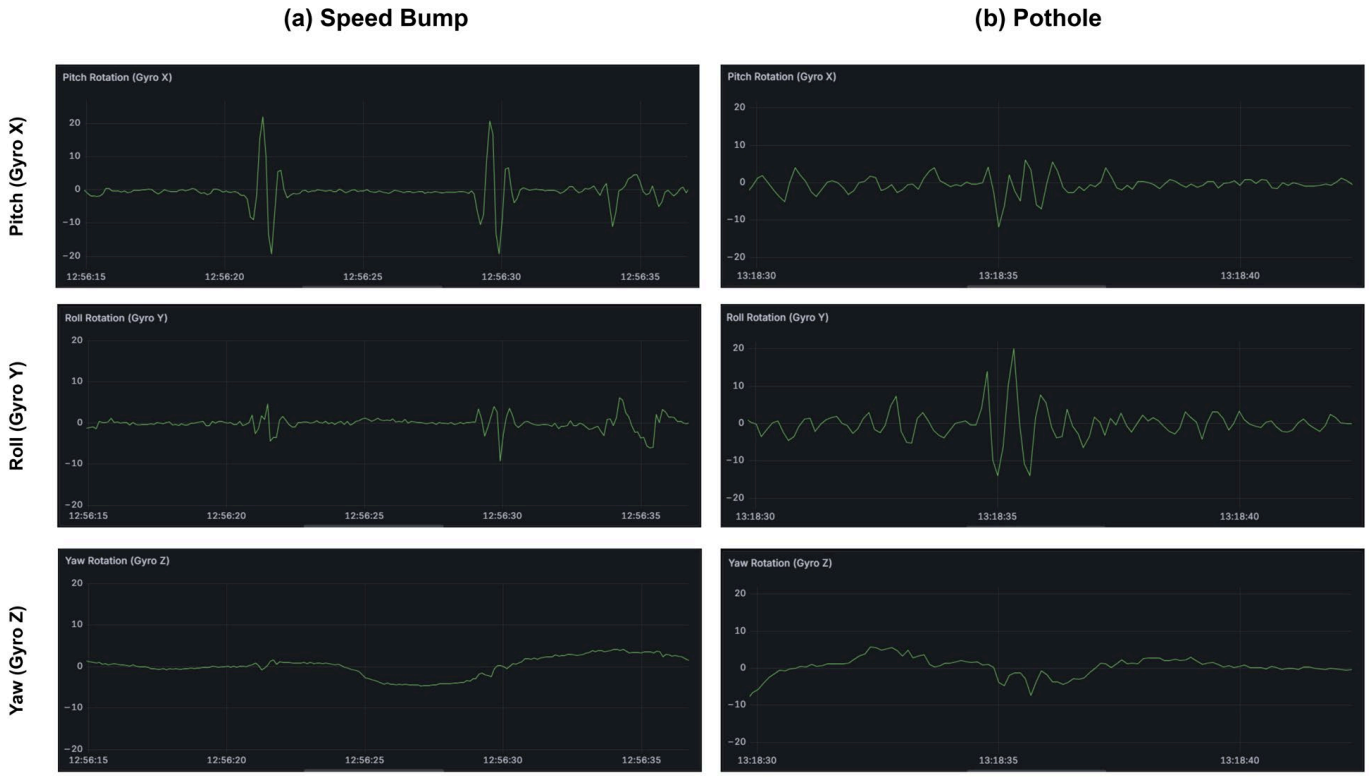

Figure 14. Gyroscope responses of SN #1 during (**a**) a speed bump and (**b**) a pothole event.

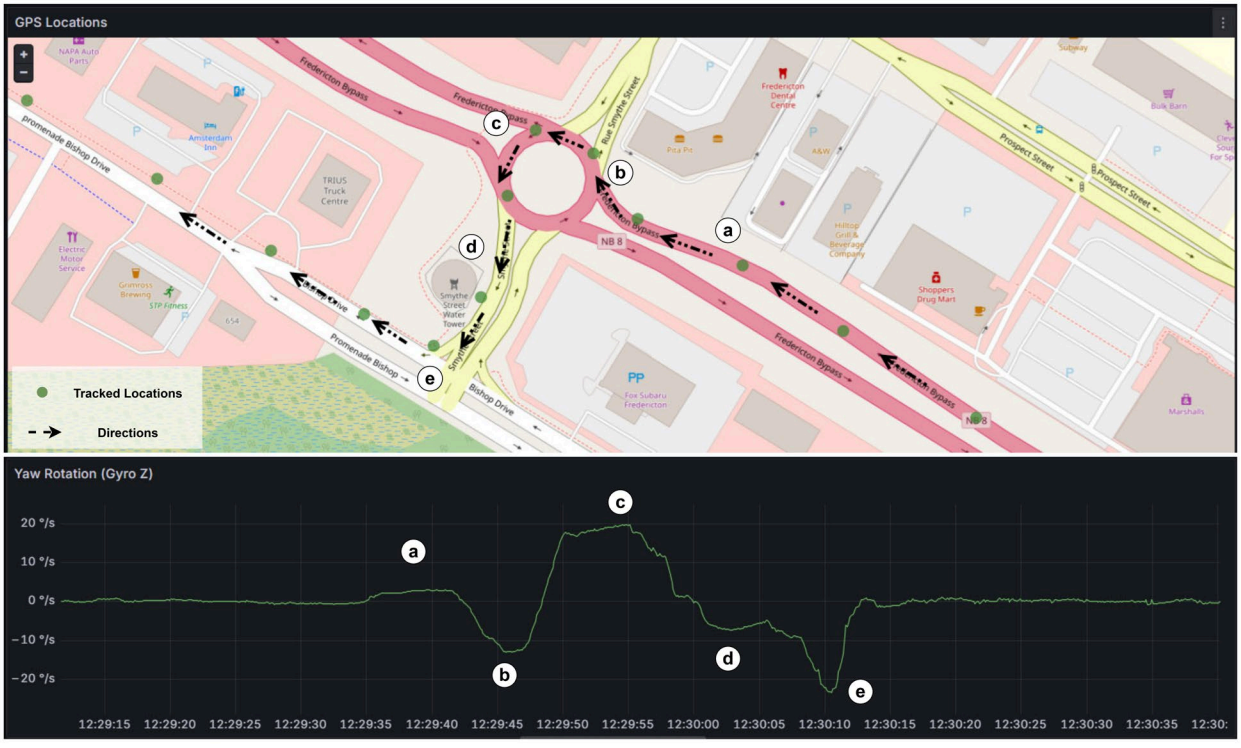

Figure 15. Yaw rotation coupled with GPS data showing vehicle maneuvers through a roundabout.

Other driver-induced events can also be identified from longitudinal acceleration (Y-axis). Large positive spikes indicate rapid acceleration, while large negative spikes correspond to harsh braking [43]. Although no such aggressive behaviors were observed in this experiment (conducted under urban conditions), the system's continuous speed

tracking provides additional context for detecting and classifying these behaviors in more diverse driving scenarios.

To further explore automated event segmentation, a rule-based heuristic pipeline was developed. In this approach, gyroscope signals were smoothed using rolling averages, and baseline motion trends were estimated dynamically with associated standard deviations. Event saliency was quantified through residual energy calculations, and candidate events were extracted via peak detection, constrained by heuristic thresholds and minimum inter-peak distances to reduce false positives. Using this method, the system detected 31 bumps, 114 potholes, and 67 turns/lane-change events. Nearly all observer-noted events, as well as those verifiable by GPS, were successfully captured, indicating the practicality of this approach for automated event detection. However, numerous additional events were also flagged, underscoring the need for refinement of thresholds and multi-sensor validation to improve accuracy. Figure 16 illustrates three representative events detected using this pipeline: the pothole and speed bump previously identified in Figure 10 and highlighted in Figure 14, and the roundabout turn shown in Figure 15.

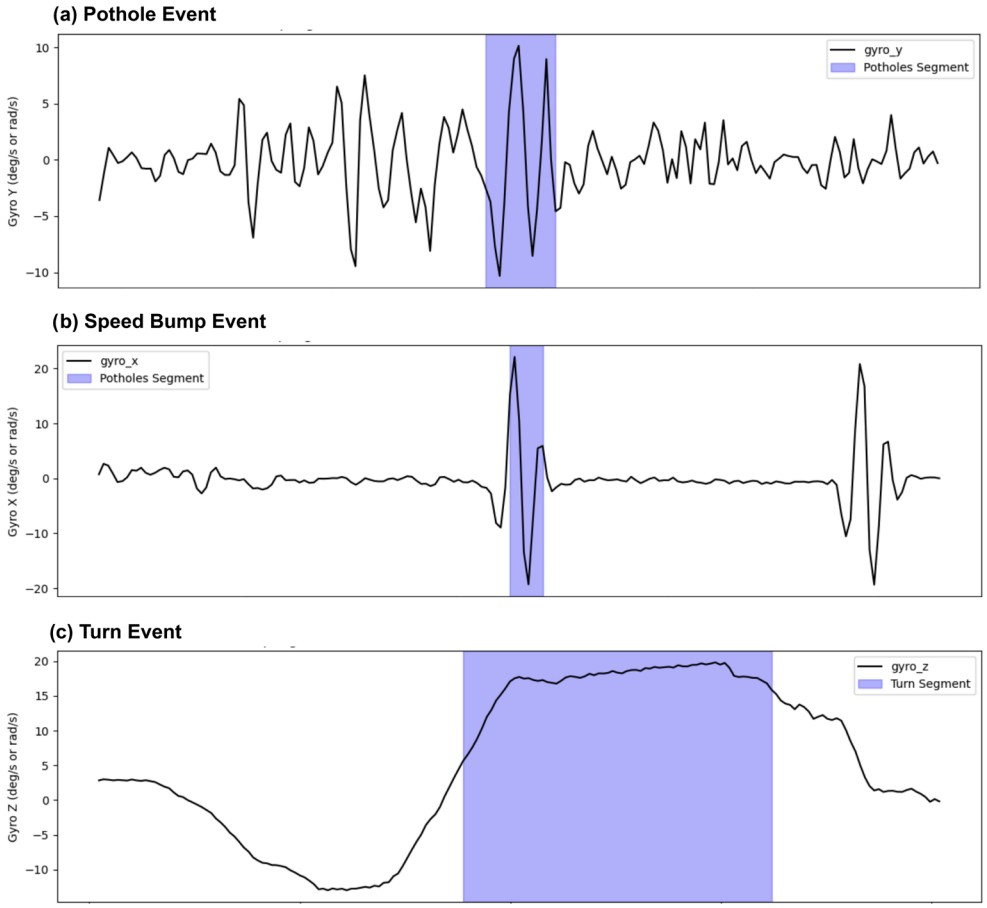

Figure 16. Examples of detected events using the heuristic method: (**a**) pothole, (**b**) speed bump, and (**c**) turn.

7. Conclusions

This study developed and validated a GPS-integrated IoT framework for real-time monitoring of prefabricated modules during transportation. The results demonstrate that a low-cost network of wireless sensing nodes, combined with a cellular-enabled gateway and containerized cloud services, can deliver reliable, loss-tolerant data acquisition and transmission under real-world conditions. Field experiments confirmed that vertical accelerations serve as the most sensitive diagnostic channel for detecting road-induced shocks,

while orientation-specific gyroscope readings effectively differentiate driver maneuvers from structural responses. By coupling these measurements with GPS coordinates, the framework enables precise localization of critical events, such as potholes, speed bumps, and unsafe handling practices, along specific route segments, offering actionable insights for targeted inspection and maintenance.

This work makes three key contributions to modular transport monitoring. First, it advances beyond conventional local data logging by implementing a fully integrated, real-time IoT architecture that streams synchronized multi-node data to the cloud, with onboard buffering and recovery logic ensuring resilience to connectivity interruptions. Second, it enhances structural monitoring with geospatial context, fusing IMU data with GPS trajectories to enable event localization, route-segment risk analysis, and transparent attribution of transport-induced impacts. Third, it demonstrates a practical, scalable, and cost-effective deployment by addressing key implementation challenges, including dynamic node–gateway pairing, real-time edge time-stamping, automated axis reorientation in the cloud, optimized data throughput, and LTE connectivity reliability, validated through a comprehensive 800 km field experiment.

At the same time, several limitations should be acknowledged. The current validation was conducted on a scaled prototype rather than a full-size modular unit, limiting the generalizability of dynamic response results to heavier and stiffer modules. Field testing was restricted primarily to urban and semi-urban routes using modern vehicle suspensions under relatively mild conditions, leaving more extreme loading scenarios unaddressed. Additionally, the event detection pipeline relies on heuristic thresholds, which may require recalibration for different test scenarios, and long-term factors such as sensor drift and temperature effects were not investigated.

Future work should address these limitations by deploying the framework on full-scale modular units across diverse transport conditions and incorporating additional sensing nodes to capture distributed responses more comprehensively. To truly quantify comparative advantages, a parallel effort must establish community-wide, standardized protocols for sensor placement, data processing, and reporting benchmarks. Transitioning from heuristic-based detection to labeled data-driven machine learning models will improve event classification robustness and generalizability. Moreover, integrating closed-loop feedback mechanisms, adaptive sampling strategies, and energy-efficient communication protocols will enhance scalability for fleet-wide deployment. Finally, tighter integration with logistics planning and scheduling systems could transform this framework into a decision-support tool that proactively mitigates risks and optimizes transport operations. Collectively, this work establishes a foundation for a unified digital ecosystem that integrates structural health monitoring with logistics intelligence, advancing the safety, resilience, and operational efficiency of modular construction transportation.

Author Contributions: Conceptualization, S.M., A.R., S.J.A. and Z.L.; methodology, S.M. and A.R.; software, S.M. and A.R.; validation, S.M. and A.R.; formal analysis, S.M. and A.R.; investigation, S.M. and A.R.; resources, H.C. and Z.L.; data curation, S.M. and A.R.; writing—original draft preparation, S.M. and A.R.; writing—review and editing, S.J.A., H.C. and Z.L.; visualization, S.M. and A.R.; supervision, H.C. and Z.L. All authors have read and agreed to the published version of the manuscript.

Funding: This work was supported by the Natural Sciences and Engineering Research Council of Canada (NSERC) through a Discovery Grant (RGPIN-2020-04126), as well as by the research funding for the OSCO Research Chair in Off-site Construction at the Off-site Construction Research Centre (OCRC), University of New Brunswick.

Data Availability Statement: Some or all data, models, or codes that support the findings of this study are available from the corresponding author upon reasonable request.

Acknowledgments: The authors thank the Off-site Construction Research Center (OCRC) and the Analytics Everywhere Research Lab for their support of this research.

Conflicts of Interest: The authors declare no conflict of interest.

References

1. Boadu, E.F.; Wang, C.C.; Sunindijo, R.Y. Characteristics of the Construction Industry in Developing Countries and Its Implications for Health and Safety: An Exploratory Study in Ghana. *Int. J. Environ. Res. Public Health* **2020**, *17*, 4110. [CrossRef] [PubMed]
2. Aghajamali, K.; Metvaei, S.; Suliman, A.; Lei, Z.; Chen, Q. Development of a Prefabricated Construction Productivity Estimation Model through BIM and Data Augmentation Processes. *Constr. Manag. Econ.* **2024**, *43*, 340–359. [CrossRef]
3. Lei, Z.; Chen, Q.; Altaf, M.S.; Cao, K. Defining Information Requirements for Off-Site Construction Management: An Industry Case Study from Canada. *J. Constr. Eng. Manag.* **2024**, *150*, 05024014. [CrossRef]
4. Bakhshi, S.; Chenaghlou, M.R.; Pour Rahimian, F.; Edwards, D.J.; Dawood, N. Integrated BIM and DfMA Parametric and Algorithmic Design Based Collaboration for Supporting Client Engagement within Offsite Construction. *Autom. Constr.* **2022**, *133*, 104015. [CrossRef]
5. Hao, J.L.; Cheng, B.; Lu, W.; Xu, J.; Wang, J.; Bu, W.; Guo, Z. Carbon Emission Reduction in Prefabrication Construction during Materialization Stage: A BIM-Based Life-Cycle Assessment Approach. *Sci. Total Environ.* **2020**, *723*, 137870. [CrossRef]
6. He, R.; Li, M.; Gan, V.J.L.; Ma, J. BIM-Enabled Computerized Design and Digital Fabrication of Industrialized Buildings: A Case Study. *J. Clean. Prod.* **2021**, *278*, 123505. [CrossRef]
7. Metvaei, S.; Aghajamali, K.; Chen, Q.; Lei, Z. Developing a BIM-Enabled Robotic Manufacturing Framework to Facilitate Mass Customization of Prefabricated Buildings. *Comput. Ind.* **2025**, *164*, 104201. [CrossRef]
8. Aghajamali, K.; Lemouchi, R.; Rahimi, A.; Metvaei, S.; Bouferguene, A.; Lei, Z. Enhancing Safety and Efficiency in Crane Operations: Addressing Communication Challenges and Blind Lifts. In Proceedings of the 2024 Winter Simulation Conference (WSC), Orlando, FL, USA, 15–18 December 2024; pp. 1–11.
9. Aghajamali, K.; Rahimi, A.; Metvaei, S.; Lei, Z.; Chen, Q.; Suliman, A.; Pirzad, A. Production Planning with an Enriched BIM-Based Heuristic Construction Order Model to Improve the Efficiency of Complex Prefabricated Projects. *J. Constr. Eng. Manag.* **2025**, *in press*. [CrossRef]
10. Metvaei, S.; Aghajamali, K.; Wang, S.; Lei, Z.; Chen, Q. Integrating Design and Fabrication for Sustainable Housing: Insights from The Kopps Prototype. In Proceedings of the Transforming Construction with Off-site Methods and Technologies, Fredericton, NB, Canada, 20–22 August 2024.
11. Arshad, H.; Zayed, T. Critical Influencing Factors of Supply Chain Management for Modular Integrated Construction. *Autom. Constr.* **2022**, *144*, 104612. [CrossRef]
12. Valinejadshoubi, M.; Bagchi, A.; Moselhi, O. Damage Detection for Prefabricated Building Modules during Transportation. *Autom. Constr.* **2022**, *142*, 104466. [CrossRef]
13. Godbole, S.; Lam, N.; Mafas, M.; Fernando, S.; Gad, E.; Hashemi, J. Dynamic Loading on a Prefabricated Modular Unit of a Building during Road Transportation. *J. Build. Eng.* **2018**, *18*, 260–269. [CrossRef]
14. Arshad, H.; Zayed, T. A Multi-Sensing IoT System for MiC Module Monitoring during Logistics and Operation Phases. *Sensors* **2024**, *24*, 4900. [CrossRef]
15. Abdelmageed, S.; Abdelkhalek, S.; Hussien, M.; Zayed, T. A Hybrid Simulation Model for Modules Installation in Modular Integrated Construction Projects. *Int. J. Constr. Manag.* **2024**, *24*, 1407–1418. [CrossRef]
16. Arshad, H.; Zayed, T.; Bakhtawar, B.; Chen, A.; Li, H. Damage Assessment of Modular Integrated Construction during Transport and Assembly Using a Hybrid CNN–Gated Recurrent Unit Model. *Autom. Constr.* **2025**, *174*, 106136. [CrossRef]
17. Smith, I.; Asiz, A.; Gupta, G. *High Performance Modular Wood Construction Systems*; Wood Science Technology Centre: Fredericton, NB, Canada, 2007; pp. 1–155.
18. Mazloom, S.; Assi, R. Estimation of Vertical Peak Floor Acceleration Demands in Elastic RC Moment-Resisting Frame Buildings. *J. Earthq. Eng.* **2023**, *27*, 3753–3785. [CrossRef]
19. Ditommaso, R.; Mucciarelli, M.; Ponzo, F.C. Analysis of Non-Stationary Structural Systems by Using a Band-Variable Filter. *Bull. Earthq. Eng.* **2012**, *10*, 895–911. [CrossRef]
20. Worden, K.; Baldacchino, T.; Rowson, J.; Cross, E.J. Some Recent Developments in SHM Based on Nonstationary Time Series Analysis. *Proc. IEEE* **2016**, *104*, 1589–1603. [CrossRef]
21. Duggal, R.; Gupta, N.; Pandya, A.; Mahajan, P.; Sharma, K.; Kaundal, T.; Angra, P. Building Structural Analysis Based Internet of Things Network Assisted Earthquake Detection. *Internet Things* **2022**, *19*, 100561. [CrossRef]

22. Khayam, S.U.; Won, J.; Shin, J.; Park, J.; Park, J.-W. Monitoring Precast Structures During Transportation Using a Portable Sensing System. *Autom. Constr.* **2023**, *145*, 104639. [CrossRef]
23. Song, S.H.; Choi, J.O.; Cho, H. Transportation-Induced Impact on a Prefinished Volumetric Modular House Using Trailer Bogie: Case Study. *J. Constr. Eng. Manag.* **2024**, *150*, 05024007. [CrossRef]
24. Broer, A.A.R.; Benedictus, R.; Zarouchas, D. The Need for Multi-Sensor Data Fusion in Structural Health Monitoring of Composite Aircraft Structures. *Aerospace* **2022**, *9*, 183. [CrossRef]
25. Alsakka, F.; Yu, H.; El-Chami, I.; Hamzeh, F.; Al-Hussein, M. Digital Twin for Production Estimation, Scheduling and Real-Time Monitoring in Offsite Construction. *Comput. Ind. Eng.* **2024**, *191*, 110173. [CrossRef]
26. Zhong, R.Y.; Peng, Y.; Xue, F.; Fang, J.; Zou, W.; Luo, H.; Thomas Ng, S.; Lu, W.; Shen, G.Q.P.; Huang, G.Q. Prefabricated Construction Enabled by the Internet-of-Things. *Autom. Constr.* **2017**, *76*, 59–70. [CrossRef]
27. Li, C.Z.; Xue, F.; Li, X.; Hong, J.; Shen, G.Q. An Internet of Things-Enabled BIM Platform for on-Site Assembly Services in Prefabricated Construction. *Autom. Constr.* **2018**, *89*, 146–161. [CrossRef]
28. Zhai, Y.; Chen, K.; Zhou, J.X.; Cao, J.; Lyu, Z.; Jin, X.; Shen, G.Q.P.; Lu, W.; Huang, G.Q. An Internet of Things-Enabled BIM Platform for Modular Integrated Construction: A Case Study in Hong Kong. *Adv. Eng. Inform.* **2019**, *42*, 100997. [CrossRef]
29. Chen, K.; Xu, G.; Xue, F.; Zhong, R.Y.; Liu, D.; Lu, W. A Physical Internet-Enabled Building Information Modelling System for Prefabricated Construction. *Int. J. Comput. Integr. Manuf.* **2018**, *31*, 349–361. [CrossRef]
30. Zhao, L.; Liu, Z.; Mbachu, J. Development of Intelligent Prefabs Using IoT Technology to Improve the Performance of Prefabricated Construction Projects. *Sensors* **2019**, *19*, 4131. [CrossRef]
31. Xu, G.; Li, M.; Chen, C.-H.; Wei, Y. Cloud Asset-Enabled Integrated IoT Platform for Lean Prefabricated Construction. *Autom. Constr.* **2018**, *93*, 123–134. [CrossRef]
32. Xu, G.; Li, M.; Luo, L.; Chen, C.-H.; Huang, G.Q. Cloud-Based Fleet Management for Prefabrication Transportation. *Enterp. Inf. Syst.* **2019**, *13*, 87–106. [CrossRef]
33. Mao, C.; Tao, X.; Yang, H.; Chen, R.; Liu, G. Real-Time Carbon Emissions Monitoring Tool for Prefabricated Construction: An IoT-Based System Framework. In Proceedings of the International Conference on Construction and Real Estate Management, Charleston, SC, USA, 9–10 August 2018; pp. 121–127. [CrossRef]
34. Lee, D.; Lee, S. Digital Twin for Supply Chain Coordination in Modular Construction. *Appl. Sci.* **2021**, *11*, 5909. [CrossRef]
35. Mardanshahi, A.; Sreekumar, A.; Yang, X.; Barman, S.K.; Chronopoulos, D. Sensing Techniques for Structural Health Monitoring: A State-of-the-Art Review on Performance Criteria and New-Generation Technologies. *Sensors* **2025**, *25*, 1424. [CrossRef] [PubMed]
36. Güemes, A.; Fernandez-Lopez, A.; Pozo, A.R.; Sierra-Pérez, J. Structural Health Monitoring for Advanced Composite Structures: A Review. *J. Compos. Sci.* **2020**, *4*, 13. [CrossRef]
37. Cawley, P. Structural Health Monitoring: Closing the Gap between Research and Industrial Deployment. *Struct. Health Monit.* **2018**, *17*, 1225–1244. [CrossRef]
38. Gómez, J.; Casas, J.R.; Villalba, S. Structural Health Monitoring with Distributed Optical Fiber Sensors of Tunnel Lining Affected by Nearby Construction Activity. *Autom. Constr.* **2020**, *117*, 103261. [CrossRef]
39. Godarzi, N.; Hejazi, F. A Review of Health Monitoring and Model Updating of Vibration Dissipation Systems in Structures. *CivilEng* **2025**, *6*, 3. [CrossRef]
40. Popescu, T.D.; Aiordachioaie, D. Fault Detection of Rolling Element Bearings Using Optimal Segmentation of Vibrating Signals. *Mech. Syst. Signal Process.* **2019**, *116*, 370–391. [CrossRef]
41. Azimi, M.; Eslamlou, A.D.; Pekcan, G. Data-Driven Structural Health Monitoring and Damage Detection through Deep Learning: State-of-the-Art Review. *Sensors* **2020**, *20*, 2778. [CrossRef]
42. Chen, D.; Cho, K.-T.; Han, S.; Jin, Z.; Shin, K.G. Invisible Sensing of Vehicle Steering with Smartphones. In Proceedings of the 13th Annual International Conference on Mobile Systems, Applications, and Services, Florence, Italy, 18–25 May 2015; pp. 1–13.
43. Kovaceva, J.; Isaksson-Hellman, I.; Murgovski, N. Identification of Aggressive Driving from Naturalistic Data in Car-Following Situations. *J. Saf. Res.* **2020**, *73*, 225–234. [CrossRef]
44. Singh, V.; Chander, D.; Chhaparia, U.; Raman, B. SafeStreet: An Automated Road Anomaly Detection and Early-Warning System Using Mobile Crowdsensing. In Proceedings of the 2018 10th International Conference on Communication Systems & Networks (COMSNETS), Bengaluru, India, 3–7 January 2018; pp. 549–552.
45. Menegazzo, J.; von Wangenheim, A. Vehicular Perception Based on Inertial Sensing: A Structured Mapping of Approaches and Methods. *SN Comput. Sci.* **2020**, *1*, 255. [CrossRef]
46. Khandakar, A.; Michelson, D.G.; Naznine, M.; Salam, A.; Nahiduzzaman, M.; Khan, K.M.; Nagaratnam Suganthan, P.; Arselene Ayari, M.; Menouar, H.; Haider, J. Harnessing Smartphone Sensors for Enhanced Road Safety: A Comprehensive Dataset and Review. *Sci. Data* **2025**, *12*, 418. [CrossRef]
47. Scuro, C.; Lamonaca, F.; Porzio, S.; Milani, G.; Olivito, R.S. Internet of Things (IoT) for Masonry Structural Health Monitoring (SHM): Overview and Examples of Innovative Systems. *Constr. Build. Mater.* **2021**, *290*, 123092. [CrossRef]

48. Chilamkurthy, N.S.; Pandey, O.J.; Ghosh, A.; Cenkeramaddi, L.R.; Dai, H.-N. Low-Power Wide-Area Networks: A Broad Overview of Its Different Aspects. *IEEE Access* **2022**, *10*, 81926–81959. [CrossRef]
49. Rahimi Azghadi, S.A.; Aghajamali, K.; Wachowicz, M.; Palma, F.; Church, I.; Cao, H. An Energy-Efficient LoRa IoT System for Water Monitoring: Lessons Learned and Use Cases. In Proceedings of the 2024 IEEE International Conference on Consumer Electronics-Asia (ICCE-Asia), Danang, Vietnam, 3–6 November 2024; pp. 1–4.
50. Buckley, T.; Ghosh, B.; Pakrashi, V. Edge Structural Health Monitoring (E-SHM) Using Low-Power Wireless Sensing. *Sensors* **2021**, *21*, 6760. [CrossRef]
51. Ahn, S.; Han, S.; Al-Hussein, M. Improvement of Transportation Cost Estimation for Prefabricated Construction Using Geo-Fence-Based Large-Scale GPS Data Feature Extraction and Support Vector Regression. *Adv. Eng. Inform.* **2020**, *43*, 101012. [CrossRef]
52. Jang, Y.; Lee, J.-M.; Son, J. Development and Application of an Integrated Management System for Off-Site Construction Projects. *Buildings* **2022**, *12*, 1063. [CrossRef]
53. Lv, W.; Meng, F.; Zhang, C.; Lv, Y.; Cao, N.; Jiang, J. A General Architecture of IoT System. In Proceedings of the 2017 IEEE International Conference on Computational Science and Engineering (CSE) and IEEE International Conference on Embedded and Ubiquitous Computing (EUC), Guangzhou, China, 21–24 July 2017; Volume 1, pp. 659–664.
54. Khan, A.; Hammerla, N.; Mellor, S.; Plötz, T. Optimising Sampling Rates for Accelerometer-Based Human Activity Recognition. *Pattern Recognit. Lett.* **2016**, *73*, 33–40. [CrossRef]
55. Kviesis, A.; Komasilovs, V.; Ozols, N.; Zacepins, A. Bee Colony Remote Monitoring Based on IoT Using ESP-NOW Protocol. *PeerJ Comput. Sci.* **2023**, *9*, e1363. [CrossRef] [PubMed]
56. InvenSense Inc. *MPU-6000 and MPU-6050 Product Specification Revision 3.4*; InvenSense Inc.: Sunnyvale, CA, USA, 2013.
57. Manso, M.; Bezzeghoud, M. On-Site Sensor Noise Evaluation and Detectability in Low Cost Accelerometers. In Proceedings of the SENSORNETS, Virtual, 9–10 February 2021; pp. 100–106.
58. Analog Devices. ADXL354 Datasheet and Product Info. Available online: https://www.analog.com/en/products/adxl354.html (accessed on 7 November 2025).
59. Hashmi, M.U.; Labidi, W.; Bušić, A.; Elayoubi, S.-E.; Chahed, T. Long-Term Revenue Estimation for Battery Performing Arbitrage and Ancillary Services. In Proceedings of the 2018 IEEE International Conference on Communications, Control, and Computing Technologies for Smart Grids (SmartGridComm), Aalborg, Denmark, 29–31 October 2018; IEEE: New York, NY, USA; pp. 1–7.
60. Innella, F.; Bai, Y.; Zhu, Z. Acceleration Responses of Building Modules during Road Transportation. *Eng. Struct.* **2020**, *210*, 110398. [CrossRef]
61. Federal Motor Carrier Safety Administration. *Cargo Securement Rules*; Federal Motor Carrier Safety Administration: Washington, DC, USA, 2014.
62. Shtayat, A.; Moridpour, S.; Best, B.; Daoud, H. Application of Noise-Cancelling and Smoothing Techniques in Road Pavement Vibration Monitoring Data. *Int. J. Transp. Sci. Technol.* **2024**, *14*, 110–119. [CrossRef]
63. de Almeida Cardoso, R.; Cury, A.; Barbosa, F. Automated Real-Time Damage Detection Strategy Using Raw Dynamic Measurements. *Eng. Struct.* **2019**, *196*, 109364. [CrossRef]
64. Long, M.T.; Rouillard, V.; Lamb, M.J.; Sek, M.A. Characterising Heave, Pitch, and Roll Motion of Road Vehicles with Principal Component and Frequency Analysis. *Packag. Technol. Sci.* **2018**, *31*, 3–13. [CrossRef]
65. Singh, B.S.B.; Rai, S. An ML-Based ERA Algorithm for Estimation of Modes Utilizing PMU Measurements. In Proceedings of the 2022 3rd International Conference for Emerging Technology (INCET), Belgaum, India, 27–29 May 2022; IEEE: New York, NY, USA, 2022; pp. 1–5.